Dalton Transactions

ROYAL SOCIETY OF CHEMISTRY

PAPER

View Article Online
View Journal | View Issue

Cite this: *Dalton Trans.*, 2024, **53**, 3836

Cobalt(III)-containing penta-dentate "helmet"-type phthalogens: synthesis, solid-state structures and their thermal and electrochemical characterization†

Rasha K. Al-Shewiki,[a] Saddam Weheabby,[b] Nell Uhlig,[a] Marcus Korb,[c] Tom Pester,[d] Stefan Zahn,[e] S. Grecchi,[f] P. R. Mussini,[f] Tobias Rüffer *[a] and Heinrich Lang[g]

Treatment of unsubstituted and substituted phthalonitrile (**1a–d**) with appropriate equivalents of sodium methoxide and ammonia afforded the corresponding 1,3-diiminoisoindolines (**2a–d**), which were converted to cobalt(III)-containing penta-dentate "helmet"-type phthalogens (**3a–d**) by the reaction with $CoCl_2 \cdot 6H_2O$ as templating agent in the inert solvent 1,2,4-trichlorobenzene. The identities of **2a–d** and **3a–d** were established by elemental analysis, infrared spectroscopy (IR), nuclear magnetic resonance (NMR), and electrospray ionization mass spectrometry (ESI-MS). A computational study was performed to determine the most stable tautomeric form of **2a–c** in the gas phase. The solid-state structures of **2b** and **2c** were determined by single crystal X-ray diffraction (SC-XRD) studies to confirm their existence in the stereoisomeric *anti*-form, which is aligned with quantum chemical computations. SC-XRD studies of **3a** and **3b** revealed a slightly distorted octahedral geometry around the Co^{III} ions which are coordinated by five N-donor atoms and one extra co-ligand, resulting in a coordination environment of CoN_5Cl (**3a**) and CoN_5O (**3b**), respectively. The thermal stabilities of **2a–d** and **3a–d** were investigated by thermogravimetric analysis (TGA) in the temperature range of 40–500 °C and 40–800 °C, respectively, revealing that **3a–d** were converted to the parent cobalt(II)-containing phthalocyanines (**4a–d**), which was verified independently by furnace heating experiments. Moreover, the electrochemical behavior of **3a** was studied exemplarily for the phthalogens by cyclic voltammetry and square wave voltammetry. This study showed that **4a** (CoPc) is formed irreversibly by reducing **3a** electrochemically.

Received 25th November 2023,
Accepted 24th January 2024

DOI: 10.1039/d3dt03950a

rsc.li/dalton

Introduction

Within the large family of porphyrinoids, (metallo)phthalocyanines (MPcs) enjoy a privileged position mainly due to their distinctive photophysical, structural, electronic, magnetic and catalytic properties combined with an exceptionally high thermal and chemical stability.[1,2] They found numerous applications in different fields, including nonlinear optics,[3] optical recording media,[4] light harvesting systems,[5] semiconductors,[6] chemical sensors,[7] photodynamic therapy[8] and catalysis.[9]

Phthalogens, as displayed in Fig. 1, are another member of the large porphyrinoid family and can be used, for example, to produce MPcs either by thermal or photochemical treatment, or by electrochemical reduction.[10–12] Phthalogens possess different chemical and physical properties compared to MPcs which is due to skeletal modification resulting in the loss of the aromaticity of the latter.[11] The already known phthalogens can be classified according to a recent review by some of us[11]

[a]*Chemnitz University of Technology, Department of Inorganic Chemistry, Strasse der Nationen 62, 09107 Chemnitz, Germany. E-mail: tobias.rueffer@chemie.tu-chemnitz.de*
[b]*Chemnitz University of Technology, Measurement and Sensor Technology, 09126 Chemnitz, Germany*
[c]*University of Western Australia, School of Molecular Sciences, M310, 6009 Perth, WA, Australia*
[d]*Chemnitz University of Technology, Department of Organic Chemistry, Strasse der Nationen 62, 09111 Chemnitz, Germany*
[e]*Leibniz Institute of Surface Engineering (IOM), Permoserstraße 15, 04318 Leipzig, Germany*
[f]*University of Milan, Department of Chemistry, Via Golgi 19, 20133 Milano, Italy*
[g]*Research Center for Materials, Architectures and Integration of Nano-membranes (MAIN) Research Group Organometallic Chemistry, Technische Universität Chemnitz Rosenbergstraße 6, 09126 Chemnitz, Germany*

†Electronic supplementary information (ESI) available: Experimental details for synthesis of **2a–d**, **3a–d** and **4a–d**, characterization data (^1H,$^{13}C\{^1H\}$ and 2D NMR, ESI-MS, IR spectra, and UV/Vis), crystal and structural refinement data. CCDC 2298395 (**2b**), 2298396 (**2c**), 2298397 (**3a**), 2298398 (**3b**) and 2298399 (**4a**). For ESI and crystallographic data in CIF or other electronic format see DOI: https://doi.org/10.1039/d3dt03950a

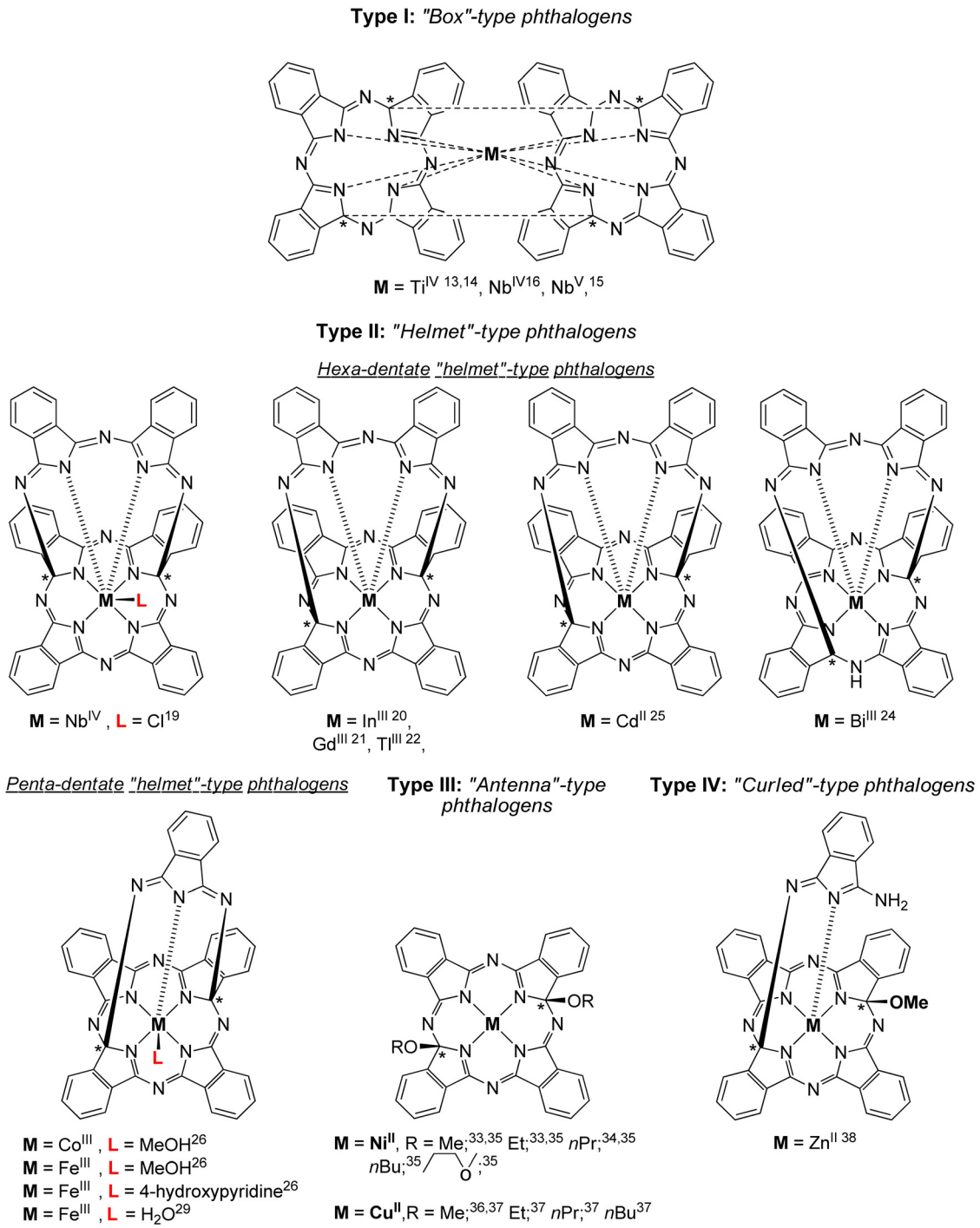

Fig. 1 Chemical structures of crystallographically characterized phthalogens.[11] The sign * indicate asymmetrically substituted carbon atoms but refer to racemic mixtures.

into four types: (i) "box"-type phthalogens (**Type I**),[13–18] (ii) "helmet"-type phthalogens (**Type II**),[19–32] (iii) "antenna"-type phthalogens (**Type III**)[33–37] and (iv) "curled"-type phthalogens (**Type IV**),[38] *cf.* Fig. 1. The first example of a crystallographically characterized phthalogen was reported by Ercolani and co-workers in 1990,[13] and later in 1998[14] for a **Type I** phthalogen (Fig. 1). The molecular structure determination revealed that **Type 1** phthalogens have a sandwich-type structure with the metal ion in the centre of the molecule and the two ligands 'stapled' together by two interligand C–C σ-bonds, leading to the formation of sp^3 hybridized and chiral carbon atoms indicated with (*) in Fig. 1. Due to the presence of the interligand σ-bonds both the planarity and resonance of the two formally fused MPcs got lost.[13–18]

The first example of a hexadentate **Type II**[19] "helmet"-type phthalogen was reported in 1990 by Strähle and Gingl, in which two carbon atoms of the inner skeleton are bonded covalently to a 3,3′-iminobis(1-isoindolylideneamino) unit.[19] As discussed before, this interrupts the resonance within the inner macrocycle ring and aromaticity got lost.[19]

Within **Type II** phthalogens the functionalized ligand act as a hexadentate one (by six isoindole-nitrogen donor atoms), while a chloride ion in the 7th position completes the coordination sphere of metal ions with higher charge, *cf.* Fig. 1.[19] Further examples of **Type II** phthalogens with M = In^{III},[20] Gd^{III},[21] Tl^{III},[22] and Cd^{II},[25] on the one, and with Bi^{III},[24] on the other hand (Fig. 1) were reported as well. Furthermore, a Nb^{IV} containing representative with the inner skeleton bridged at different positions was observed as well.[14–16]

The group of McGaff contributed with two further types of crystallographically characterized phthalogens, namely the one of **Type II** (pentadentate bicyclic "Helmet"-type phthalogen) and **Type III** (Fig. 1).[19–37] In the case of the **Type III** representatives[19–32] the modification of the ligand took place by incorporation of two alkoxy groups at the inner skeleton. As reported before for the other phthalogens, that resulted in rehybridization of the respective carbon atoms from sp^2 to sp^3. Once again, the planarity of the formally phthalocyaninato core and its π-conjugation is lost, the latter is proven by the disappearance of the Q band in UV/Vis spectra.[33] In case of the **Type II** pentadentate bicyclic "helmet"-type phthalogen,[26] the ligand consist of five isoindoline units which coordinates to the trivalent metal ions Fe^{III} and Co^{III} by five N-donor atoms, one from each isoindoline unit. As their synthesis made use of Fe^{II} or Co^{II} salts as starting compounds a one-electron oxidation did obviously occur, and it seems as if this oxidation is a prerequisite for the formation of **Type II** compounds. So far, no Type **II** representative possessing a bivalent metal ion has been reported. The coordination sphere around the trivalent metal ions is fulfilled by an additional donor as a coordinating methanol, water or 4-hydroxypyridine molecule (Fig. 1).[26] The iron(III) containing compounds attracted attention through the years due to their close relevance to biological activities involving heme proteins[27–30] and have been used in oxidation catalysis to generate alcohols from cycloalkanes,[27,30] epoxides from olefins[28] and ketones and aldehydes from unactivated non-benzylic alcohols.[29] All phthalogens reported so far have been synthesized from the reaction of a metal source as templating agent and a phthalonitrile precursor.[13–38] However, another simpler synthetic route involve the direct use of 1,3-diiminoisoindoline have been reported.[10,39] Additionally, 1,3-diiminoisoindoline is also useful for the synthesis of various phthalocyanine analogues, such as subphthalocyanine,[40] hemiporphyrazines,[41] metal chelates such as the bis(iminopyridyl)isoindoline[42] and phthalazine ligands.[43] In early 1950s, Linstead synthesized 1,3-diiminoisoindoline from the addition of liquid ammonia in a methanolic solution of phthalonitrile; the reaction mixture was heated in an autoclave for four hours to yield a beige/light green product.[39a] Later on 1,3-diiminoisoindoline was synthesized by using a catalytic amount of sodium in methanol,[10] and since then several methods have been developed for the preparation of further 1,3-diiminoisoindolines.[44]

Here we report on an novel synthetic approach to prepare 1,3-diiminoisoindolines in very high yields and on an straightforward and easy-to-follow approach to synthesize cobalt(III) containing penta-dentate "helmet" type phthalogens (**3a–d**, **Type II**) under mild conditions. The compounds were characterized by a comprehensive set of techniques, including elemental analysis, IR, NMR, ESI-MS, UV/VIS, X-ray, and TGA. The process of converting **3a–d** into the parent MPcs **4a–d** through thermal decomposition and electrochemical reduction was examined.

Results and discussion

Synthesis

In order to have suitable precursors to synthesize cobalt(III) containing penta-dentate "helmet"-type phthalogens **3a–d**, the corresponding phthalonitriles **1a–d** were first converted to the 1,3-diiminoisoindoline's **2a–d** (Scheme 1).

Compounds **2a–d** were synthesized by a one-pot method in excellent yields under mild solvothermal reaction conditions by reacting **1a–d** with five equivalents of ammonia in a methanolic solution (see ESI†). When using less than five equivalents of ammonia in methanol as solvent the yields were always lower, the reaction times became longer, and the isolated materials were not analytically pure.

The synthesis of **3a–d** included two steps: (i) the reaction of $CoCl_2{\cdot}6H_2O$ as templating agent with five equivalents of the corresponding 1,3-diiminoisoindoline's **2a–d** in 1,2,4-trichlorobenzene as an inert and high boiling solvent and (ii) recrystallization of solid reaction products from dmf. With respect to (i): the reaction temperature was raised slowly up to 200–210 °C (*cf.* Experimental section and ESI†) to avoid boil over due to release of NH_3. Stirring at that temperature was continued as long as NH_3 developed. After the NH_3 development ceased the reaction mixture was filtered off. In step (II) the filter cake was transferred into dmf and stirred for two hours. The resulting suspension was filtered again and allowed to separate purple or bluish-purple solids from an intense green coloured solution. The solid materials were identified as the cobalt(II) phthalocyanines **4a–d**, whereby further purification[39f] was needed to obtain them analytically pure (see ESI†). The green filtrate was crystallized with et_2O to obtain **3a–d** as dark-red (**3a**) or orange crystals (**3b–d**) (see ESI†). In case of **3a** no further purification was required and the crystallization afforded **3a** in form of [**3a**(HCl)(dmf)]·2dmf, while for **3b–d** complexes further purification efforts were required. Thereby, **3b** complex was purified by two subsequently performed column chromatography using CH_2Cl_2 and EtOAc as eluent; respectively, affording **3b** in form of [**3b**(dmf)]·dmf·H_2O based upon elemental analysis studies. In case of **3c**, separated orange microcrystals were noticed to be

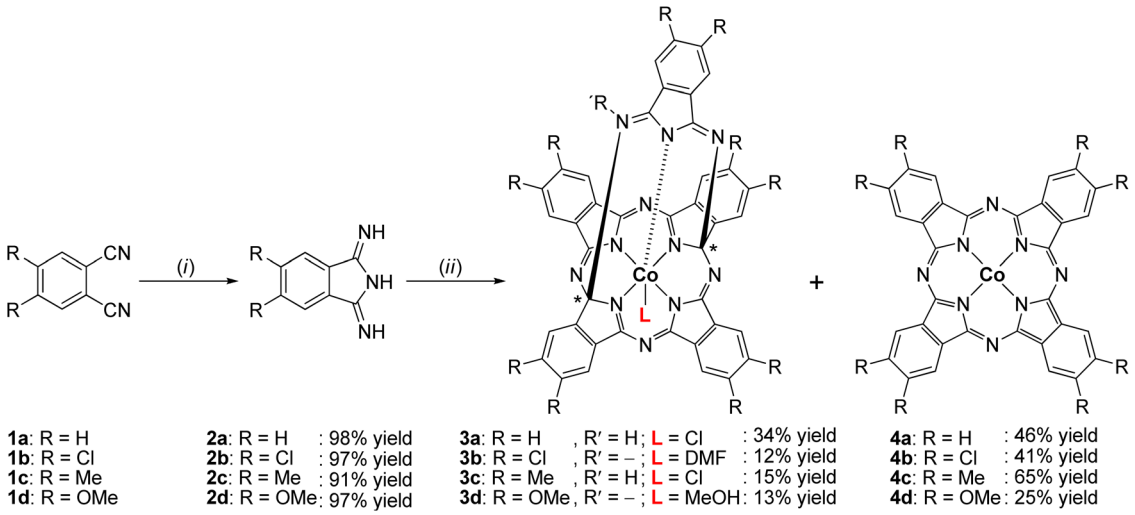

Scheme 1 Synthesis of **2a–d**, **3a–d** and **4a–d**. (i) NH_3, NaOMe, MeOH, 60–70 °C, 4 h, (ii) $CoCl_2{\cdot}6H_2O$, 1,2,4-trichlorobenzene, Δ.† Comment: **2d** was obtained as **2d**·H_2O, **3a** as [**3a**(HCl)(dmf)]·2dmf, **3b** as [**3b**(dmf)]·dmf·H_2O and as [**3b**(dmf)]·2dmf in singly crystalline form, **3c** as [**3c**(HCl)]·dmf and **3d** as [**3d**(MeOH)]·dmf.

contaminated with an undetermined colourless material, therefore it was sonicated in MeOH for 15 min to afford **3c** afforded in form of [**3c**(HCl)]·dmf. Crystals of **3d** were purified by column chromatography by using a CH_2Cl_2–MeOH mixture (ratio 3 : 1, v/v) to afford **3d** in form of [**3d**(MeOH)]·dmf (see ESI†).

In addition, another purification experiment of **3a** was performed. The obtained crystals were dissolved in a minimum amount of dichloromethane and loaded onto a short silica gel flash column. An orange band was quickly eluted when a CH_2Cl_2–MeOH mixture (ratio 3 : 1, v/v) was passed through the column. The band was collected and upon slow evaporation of the solvent mixture dark red crystals of **3a·MeOH** could be separated (see ESI†).

Characterization of 2a–d

Compounds **2a–d** have three ionizable protons (H^+) present on the imine and/or isoindoline nitrogen atoms[45] and are therefore involved in a tautomeric equilibrium between the diimino and amino-imino form (Scheme 2).

Both tautomeric forms might be involved in *syn–anti* equilibria (Scheme 2) with respect to the orientation of the =N–H hydrogen towards the aromatic ring (*syn*) or away from it (*anti*). The room temperature ^{1}H NMR spectra of **2a–d** in DMSO-d_6 confirmed the presence of mainly the C_2 symmetric diimino tautomers, while broad resonances at 8.52, 8.71, 8.37 and 8.41 ppm for the N–H protons of **2a**, **2b**, **2c** and **2d** indicate a dynamic behavior in solution (see ESI†). ESI-TOF mass-spec-

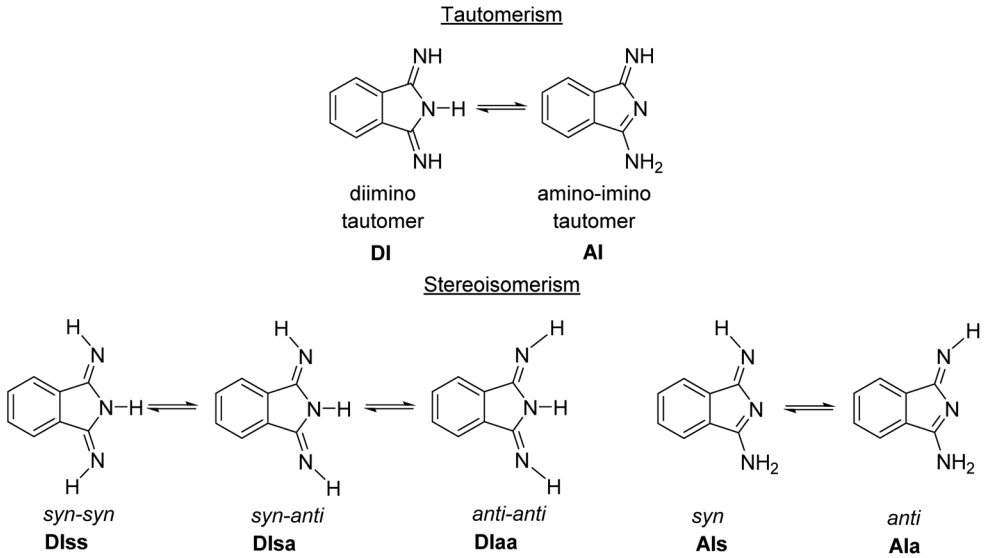

Scheme 2 Principal tautomerism and stereoisomerism in 1,3-diiminoisoindolines on example of **2a**.[45]

trometric spectra of **2a–d** showed in all cases the molecular ion peaks as basis peaks in the form of $[M + H]^+$ (see ESI†), while for **2d**, which was isolated as the adduct **2d**·H_2O, the peak of $[\mathbf{2d} + H_2O + H]^+$ was observed in addition (see ESI†). In the FT-IR spectra of **2a–d** taken from KBr pellets the intense absorption band around 2231 cm^{-1}, corresponding to the –C≡N group of phthalonitriles **1a–d**, disappeared as a further prove of their conversion to analytically pure **2a–d** (see ESI†).

Molecular and crystal structure of 2b and 2c

The single crystal X-ray crystallographic studies (SC-XRD) of **2b** and **2c** confirmed both compounds as being isomorphic and isostructural. Therefore, the following discussion will include mostly **2b**, which applies in particular to the discussion of the crystal structures. A comparison of related bond lengths of **2b** and **2c** reveals no further significant differences, while related bond angles show marginal differences only. Much likely, this is due to the formation of intermolecular interactions of **2b** and **2c**, especially by means of hydrogen bond formation, which possess a larger impact on these structural parameters than the different electronic nature of the chloro (**2b**) *vs.* the methyl (**2c**) substituents, respectively. The molecular structure of **2b** is shown in Fig. 2 as a dimer in order to visualize the importance of hydrogen bond formation. Selected bond lengths and angles, in comparison to the ones of **2c**, are summarized in Table 1, selected geometrical data of hydrogen bonds of **2b** and **2c** are given in Table 2 while Table S9† gives selected data collection and structural refinement data.

Molecular structures. Compound **2b** is observed in the solid state in the stereoisomeric *anti* form of the *amino-imino tautomer*. This is consistent with already made quantum chemical calculations[46,47] and SC-XRD studies[48,49] of other 1,3-diimino-isoindolenes which verified that the diimino tautomeric form is dominant in solution and possess lower energy compared to the *amino-imino tautomer*, which is, however, prevalent in the solid state due to formation of intermolecular hydrogen bonds.

The formal C–NH_2/N–C single bonds (d(C1–N1)/(N2–C8) = 1.308(3)/1.382(3) Å) are just marginally longer compared to the formal C=NH/C=N double bonds (d(C8–N3)/(C1–N2) = 1.282(3)/1.327(3) Å). This observation indicates the H_2N–C=N–C=NH unit of **2b** as stabilized by mesomerism, but not in resonance with the substituted benzene ring. The latter is verified by bond lengths of 1.492(3) and 1.494(3) Å for C1–C2 and C7–C8, which both corresponds well to expected values for a C–C single bond and by which the two resonant groups are separated. Both **2b** and **2c** are planar as revealed from very small root-mean-square deviations from planarity of calculated mean planes of all atoms of 0.024 and 0.022 Å, respectively, with the highest deviation from planarity observed for N2 with 0.060(5) Å for **2b** and for C9 with 0.056(8) Å for **2c**.

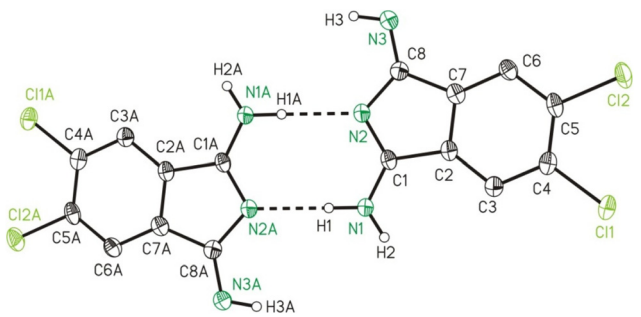

Fig. 2 ORTEP (50% probability ellipsoids) of a dimer formed by **2b** in the solid state by means of hydrogen bond formation. Symmetry code: "A" = –*x*, –*y*, –*z*.

Table 1 Selected bond lengths (Å) and bond as well as torsion angles (°) of **2b** and **2c**

Bond length			Bond angles		
	2b	**2c**		**2b**	**2c**
N1–C1	1.308(3)	1.320(5)	N1–C1–N2	123.7(2)	122.7(4)
C1–N2	1.327(3)	1.330(5)	N1–C1–C2	124.8(2)	125.2(4)
C1–C2	1.492(3)	1.477(5)	C2–C1–N2	111.4(2)	112.1(3)
N2–C8	1.382(3)	1.396(5)	C1–N2–C8	108.2(2)	107.2(3)
C8–N3	1.282(3)	1.286(5)	N2–C8–N3	126.2(2)	125.9(4)
C7–C8	1.494(3)	1.493(5)	N2–C8–C7	109.2(2)	109.0(3)
C2–C7	1.393(3)	1.381(5)	N3–C8–C7	124.5(2)	125.1(4)
C2–C3	1.384(3)	1.389(5)	C6–C7–C8	133.5(2)	133.0(3)
C3–C4	1.393(3)	1.395(5)	C6–C7–C2	120.6(2)	120.9(4)
C4–C5	1.398(4)	1.403(5)	C8–C7–C2	105.9(2)	106.1(3)
C5–C6	1.393(4)	1.397(5)	C1–C2–C7	105.3(2)	105.7(3)
C6–C7	1.380(3)	1.383(5)	C1–C2–C3	132.9(2)	133.4(4)
			C3–C2–C7	121.9(2)	121.0(3)

Table 2 Selected bond lengths (A) and angles (°) of the intermolecular hydrogen bonds of **2b** and **2c**

D–H···A[a]	D–H	H···A	D···A	D–H···A
2b:				
N1–H1···N2A[b]	0.91(3)	1.98(3)	2.891(3)	173(3)
N1C–H2C···N3[b]	0.87(3)	2.00(3)	2.848(3)	165(3)
2c:				
N1–H2···N2A	0.96(5)	1.94(5)	2.896(5)	173(4)
N1C–H1C···N3	0.99(4)	1.89(4)	2.858(4)	167(4)

[a] Symmetry codes: "A" = –*x*, –*y*, –*z*. "B" = –*x*, *y* + ½, –*z* + ½. "C" = *x*, ½ – *y*, *z* + ½. [b] For a graphical representation *cf.* Fig. S1.†

Crystal structures. In the solid state **2b** forms a 3D network due to formation of intermolecular hydrogen bonds (Table 2) and by intermolecular dispersion interactions (denoted as π-interactions). Fig. 3 displays one of the layers of **2b** formed due to intermolecular hydrogen bonds along the *b* and *c* axes. Fig. S67† displays the formation of π-interactions which are observed within these layers. Noticeable, hydrogen bond formation gives rise to layer formation only, as displayed in Fig. S68† by presenting three superimposed layers two different perspective views. The presence of π-interactions within these bands is shown exemplarily in Fig. S69† to reveal all features responsible for the network formation.

Computational investigation of 2a–c

The five possible different stereo isomers of **2a–c** (*cf.* Scheme 2) were calculated with ORCA (*cf.* Experimental

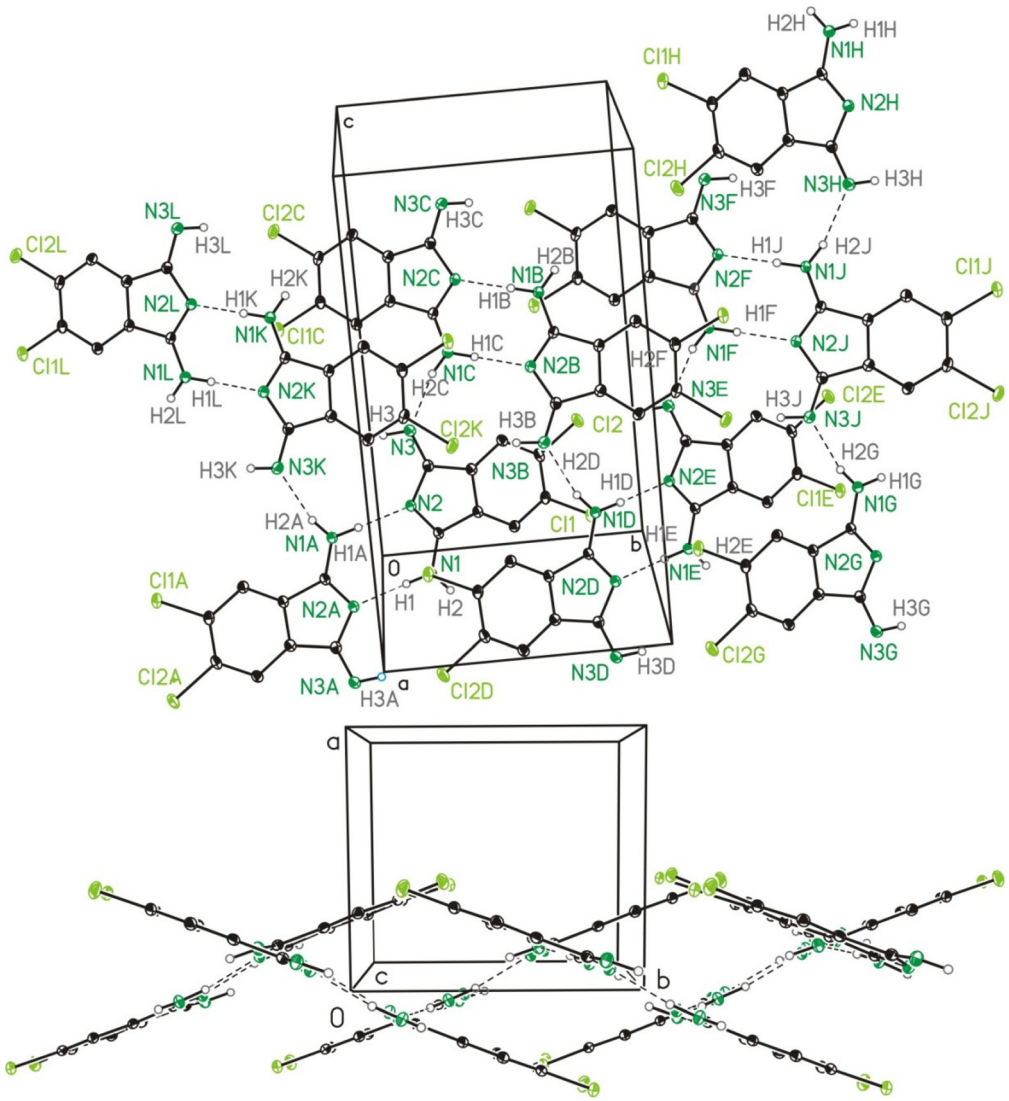

Fig. 3 ORTEP (20% probability ellipsoids) of two different perspective views on a selected part of one of the layers formed by **2b** in the solid state due to hydrogen bond formation (layer I). Dotted lines refer to intermolecular hydrogen bonds. Intermolecular π-interactions are not indicated. Symmetry codes: "A" = $-x, -y, -z$. "B" = $-x, y + \frac{1}{2}, -z + \frac{1}{2}$. "C" = $x, \frac{1}{2} - y, z + \frac{1}{2}$. "D" = $-x, 1 - y, -z$. "E" = $x, 1 + y, z$. "F" = $-x, 3/2 - y, z + \frac{1}{2}$. "G" = $-x, 2 - y, -z$. "H" = $-x, 2 - y, -z + \frac{1}{2}$. "J" = $-x, 3/2 + y, z + \frac{1}{2}$. "K" = $-x, -\frac{1}{2} + y, -z + \frac{1}{2}$. "L" = $x, -y - \frac{1}{2}, z + \frac{1}{2}$.

section) in the gas phase and in dmf solution. It was found that the *syn* isomers of the diimino tautomeric forms, namely **DIss** (Scheme 2, and Fig. 4), possess the lowest relaxed interaction energy (ΔE_{gas}) for the here investigated representatives in the gas phase (Table 3). In case of **2c** the stability of the **2c-DIss** compared to the other conformers is more pronounced, while in case of **2b** the inverse behaviour is observed. This is attributed to the electron pushing properties of the methyl groups of **2c** compared to the electron withdrawing properties of the chloro substituents of **2b**.

Considering solvation effects and thermodynamic corrections a significant decrease of the energy splitting between all conformers of **2a–c** is noticed, *cf.* ΔE_{dmf} in Table 3. Moreover, in case of **2b** the **2b-AIa** tautomer is more stable compared to the **2b-DIss** tautomer, although the difference of ΔE_{dmf} between both tautomers is small. For comparison, the reactions from the most stable monomer to two dimers, **X-D1** and **X-D2**, were investigated as well. The methyl as well as the chlorine substituent increases the stability of the investigated dimers in the gas phase (ΔG_{gas}) and in solution (ΔG_{dmf}).

Molecular structures of 3a and 3b

Single crystals of [**3a**(HCl)(dmf)]·2dmf and of [**3b**(dmf)]·2dmf were studied by SC-XRD. Data will be compared with the ones of **3a** in form of [**3a**(MeOH)]·2MeOH.[26] In the following to the fragments [**3a**(HCl)(dmf)], [**3a**(MeOH)] and [**3b**(dmf)] is referred to as **3a′**, **3aL**[26] and **3b′**. The molecular structures of **3a′** and **3b′** are shown in Fig. 5. Selected bond lengths and angles are summarized in Table 4, while Table S9† gives selected data collection and structural refinement data.

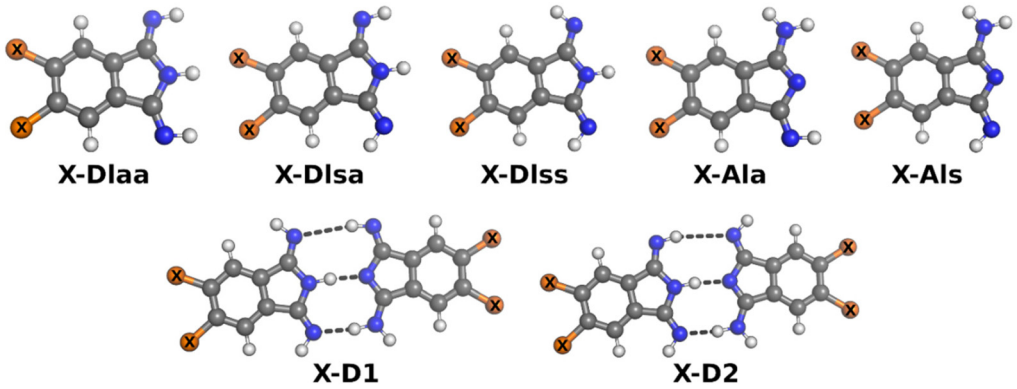

Fig. 4 Ball-and-stick-model of investigated isomers of monomers and dimers. X is H in case of **2a**, Cl in case of **2b** or Me in case of **2c**.

Table 3 Calculated energy ΔE and free reaction enthalpy difference ΔG (kJ mol^{-1}) in the gas phase and in dmf solution of isomers of **2a–c**. The most stable isomer of the monomer is set to 0 kJ mol^{-1}

Isomer	ΔE_{gas}	ΔG_{gas}	ΔE_{dmf}	ΔG_{dmf}
2a-DIaa	5.4	11.3	2.7	3.7
2a-DIsa	1.1	8.4	1.5	1.0
2a-DIss	0.0	0.0	0.0	0.0
2a-AIa	7.4	10.8	2.5	0.7
2a-AIs	23.1	26.1	5.3	6.2
H-D1	−68.8	9.7	−34.4	29.1
H-D2	−58.9	12.3	−32.2	30.5
2b-DIaa	3.8	4.1	1.0	0.9
2b-DIsa	0.4	0.0	0.3	1.8
2b-DIss	0.0	0.4	0.0	2.8
2b-AIa	5.4	2.3	0.2	0.0
2b-AIs	22.0	16.6	3.8	3.7
Cl-D1	−64.9	1.5	−37.0	23.0
Cl-D1	−61.9	1.3	−34.8	29.4
2c-DIaa	11.0	8.0	2.2	0.8
2c-DIsa	1.4	1.8	1.0	0.4
2c-DIss	0.0	0.0	0.0	0.0
2c-AIa	8.7	2.3	3.1	3.4
2c-AIs	23.6	17.6	10.6	8.2
Me-D1	−59.6	−3.5	−33.7	26.5
Me-D2	−56.1	0.2	−31.6	25.5

The Co^{III} ions of **3a′**, **3b′** and **3aL**[26] are coordinated by five N-donor atoms and by one additional co-ligand, which is in case of **3a′** an anionic chloro-ligand and in case of **3b′** and **3aL**[26] a neutral dmf and MeOH molecule, respectively (Fig. 5). The coordination setups of **3a′** (CoN_5Cl) and of **3b′**/**3aL** (CoN_5O) possess all a slightly distorted octahedral geometry as referred, for example, from bond angles between *trans*- and *cis*-bonded donor atoms ranging from 173.6(1)° (**3a′**) to 179.8(1)° (**3a′**) and from 84.88(6)° (**3aL**) to 95.9(2)° (**3b′**). Comparing related bond lengths of the CoN_5Cl and CoN_5O coordination setups with each other reveals significant differences, which can be attributed to the different nature/charge of the co-ligands. Due to the larger charge input of the anionic chloro ligand of **3a′**, which is compensated by an H^+ ion bonded to N9 (Fig. 5), the *trans*-aligned Co–N bond is substantially elongated compared to the related bonds of **3b′** and **3aL** (*d*(Co1–N10): **3a′** = 1.889(3) Å *vs.* **3b′**/**3aL** = 1.850(4)/1.858(2) Å). Furthermore, some *cis*-aligned Co–N bonds of **3a′** are significantly elongated if compared to **3b′** and **3aL** (Co1–N7 and Co1–N5, see Table 4), which is attributed to the charge input as well, although the bonds Co1–N1 and Co1–N3 of all three compounds are equal in length.

The helmet, thus the bridging fifth 1,3-diimino-isoindolene unit including the atoms N9–N11, C33–C40 (**3a′**) and additionally Cl9, Cl10 (**3b′**) is negatively charged and bonded *via* the above mentioned Co1–N10 bond to the Co^{III} ions. The helmet is bonded *via* the two covalent single bonds (see below) N9–C16/N11–C32 to the $CoC_{32}N_8H_{16}$ (**3a′**, **3aL**) or $CoC_{32}N_8Cl_8H_8$ (**3b′**) core. As a consequence, the aromaticity of these cores got lost, although **4a** (**CoPc**) and **4b** (**$CoPcCl_{10}$**) possess cores with identical sum formulas. Additionally, the carbon atoms C16 and C32 obtain a fourth different bonding partner and thus chiral information. In the here reported cases of **3a′**, **3b′** and **3aL** the solid state comprises racemates composed of the *S*,*S* and *R*,*R* enantiomers. The imprint of a chiral information onto the previous non-chiral phthalocyanin core is a unique feature common to nearly all so far reported phthalogens.[11]

In case of **3a′** the nitrogen atom N9 is protonated and involved in a hydrogen bond with one dmf molecule (Fig. 5, (*d*(N1···O3D) = 2.771(4) A; ∡(N1–H1N···O3D) = 171(4)°)), although this feature does not induce any difference into related bond lengths of **3a′** compared to **3b′** and **3aL**,[26] (Table 4). Next, selected features of the molecular structure of **3a′** shall be compared with the ones of **4a** and of **2b**. Thereby, selected bond lengths and angles of **4a** will be taken from a SC-XRD study performed along with the here reported work. Single crystals of **4a** and of many others pristine metallophthalocyanines were so far exclusively fabricated by means of physical vapour transport methods (see Table S10†) and allows to obtain (needle like) crystals with dimensions up to 20 × 1 × 1 mm. When crystallizing the filtrated and concentrated solutions directly after the synthesis of all here reported helmet type phthalogens in all cases the formation of the related CoPc's was observed. The formation of crystalline CoPc's was noticed by their extraordinary large brightness and reflectivity in single crystalline state (see Fig. S70†). Only in case of **4a**, however, the crystals were sufficiently large (up to 5 × 5 ×

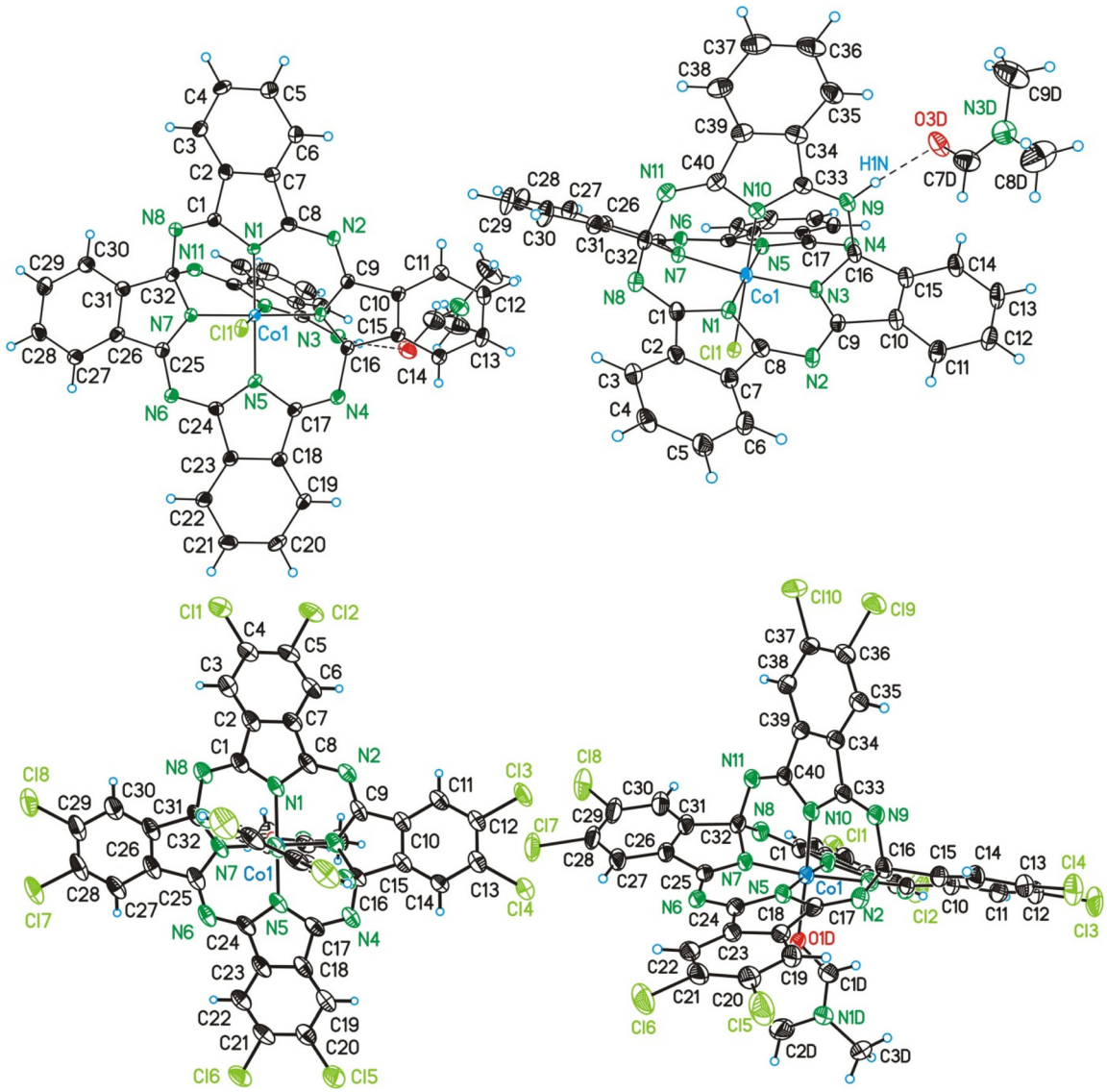

Fig. 5 ORTEP (50% probability ellipsoids) of the molecular structure of **3a′** (above) and **3b′** (below) in two different perspective views.

1 mm) for a SC-XRD study. The molecular structure of **4a** is displayed in Fig. S71, and Table S11† gives selected bond lengths, bond and torsion angles while Table S9† summarizes selected crystal and structural refinement data of **4a**. The most obvious difference between the molecular structure of **3a′** compared to the one of **4a**, beside the bridging helmet, is the non-planarity of the CoN_8C_{32} unit, which both compounds have in common. In case of **3a′** this unit has a root-mean-square deviation (rmsd) from planarity of 0.638 Å, with the highest deviation from planarity (hdp) observed for C21 with 1.197 Å which indicates severe distortion. For **4a** the rmsd from planarity amounts to 0.050 Å with a hdp of 0.092 observed for C16. Thus, as expected, **4a** is flat. For a graphical visualization of the distorted (**3a′**) *vs.* the flat geometry (**4a**) of these units Fig. 6 displays in two perspective views their overlay.

The Co–N bond lengths of **4a** (1.922(2) and 1.924(2) Å) are significantly longer compared to the ones of **3a′** (1.865(3)–1.906(3) Å), which might be attributable to the larger ionic radius of Co^{II} in square-planar *vs.* Co^{III} in distorted octahedral coordination geometry. The differences in the bond lengths and angles between **4a** and **3a′** are determined by the bridging helm, by which the atoms C16 and C32 are sp^3 hybridized. Consequently, all bonds of these two atoms to its neighbouring atoms are single bonds with bond lengths in the range between d = 1.452(2) Å (C32–N8) to 1.523(5) Å (C15–C16). The bond angles around sp^3 hybridized C16/C32 deviate substantially from the ideal 109.47° angle (range: ∡(C31–C32–N7) = 101.5(3) to ∡ (N3–C16–N4) = 116.3(3)°), although the sum of all angles around C16/C32 is with 656.4(7)/656.7(7)° very close to the value for an ideally sp^3 hybridized atom of 656.82°. Because of the solely single bond character of the bonds C16–N4/C32–N8 the other bonds involving the N atoms, namely N4–C17/N8–C1 (1.286(5)/1.289(5) Å) are classic double bonds in character. Among all other bonds of **3a′** the latter two bonds

Table 4 Selected bond lengths (Å) and angles (°) of **3a′**, **3b′** and **3aL**[26]

Bond lengths				Bond angles			
	3a	**3b**	**3aL**		**3a**	**3b**	**3aL**
Co1–N1	1.906(3)	1.899(4)	1.896(2)	N1–Co1–N3	88.9(1)	89.0(2)	89.31(7)
Co1–N3	1.865(3)	1.859(4)	1.861(2)	N1–Co1–N5	177.1(1)	174.9(2)	174.93(7)
Co1–N5	1.896(3)	1.878(4)	1.898(2)	N1–Co1–N7	91.1(1)	91.0(2)	90.72(7)
Co1–N7	1.871(3)	1.857(4)	1.854(2)	N1–Co1–N10	91.0(2)	92.6(2)	92.39(7)
Co1–N10	1.889(3)	1.850(4)	1.858(2)	N1–Co1–D	88.9(1)	87.1(2)	84.88(6)
Co1–D[a]	2.2942(9)	2.012(3)	1.998(1)	N3–Co1–N5	91.2(1)	91.4(2)	90.87(7)
C16–N9	1.495(5)	1.461(6)	1.481(3)	N3–Co1–N7	173.6(1)	173.8(2)	174.36(7)
C16–N4	1.453(5)	1.459(6)	1.465(3)	N3–Co1–N10	86.8(1)	87.0(2)	87.08(7)
C16–N3	1.466(5)	1.485(6)	1.473(3)	N3–Co1–D	93.0(1)	95.9(2)	93.67(6)
C16–C15	1.523(5)	1.522(6)	1.525(3)	N5–Co1–N7	89.1(1)	89.1(2)	89.59(7)
C32–N7	1.481(4)	1.483(7)	1.473(2)	N5–Co1–N10	91.8(2)	92.4(2)	92.39(7)
C32–N8	1.452(5)	1.458(6)	1.462(2)	N5–Co1–D	88.2(1)	87.7(2)	84.88(6)
C32–N11	1.485(5)	1.460(6)	1.479(2)	N7–Co1–N10	86.9(1)	86.8(2)	87.28(7)
C32–C31	1.518(5)	1.520(6)	1.523(3)	N7–Co1–D	93.3(1)	90.2(1)	91.97(7)
C1–C2	1.481(6)	1.489(6)	1.482(3)	N10–Co1–D	179.8(1)	177.0(2)	177.17(6)
C7–C8	1.465(5)	1.477(7)	1.479(3)	C15–C16–N3	102.4(3)	101.6(4)	102.0(2)
C9–C10	1.478(5)	1.472(7)	1.474(3)	C15–C16–N4	112.5(3)	111.5(4)	111.9(2)
C17–C18	1.485(6)	1.477(7)	1.482(3)	C15–C16–N9	109.3(3)	107.8(4)	108.1(2)
C23–C24	1.475(5)	1.477(7)	1.475(3)	N3–C16–N4	116.3(3)	113.0(4)	114.0(2)
C25–C26	1.481(5)	1.476(7)	1.472(3)	N3–C16–N9	106.7(3)	111.9(4)	111.5(2)
C33–C34	1.482(5)	1.491(6)	1.483(3)	N4–C16–N9	109.2(3)	110.7(4)	109.0(2)
C39–C40	1.481(5)	1.481(6)	1.486(3)	C31–C32–N7	101.5(3)	101.4(4)	102.2(2)
C1–N8	1.289(5)	1.276(6)	1.284(3)	C31–C32–N8	112.1(3)	111.1(4)	112.8(2)
C1–N1	1.394(5)	1.391(6)	1.407(3)	C31–C32–N11	108.9(3)	109.2(3)	107.4(2)
N1–C8	1.353(5)	1.350(5)	1.353(3)	N7–C32–N8	115.8(3)	114.7(4)	113.8(2)
C8–N2	1.324(5)	1.319(6)	1.327(3)	N7–C32–N11	111.3(3)	111.0(4)	111.6(2)
N2–C9	1.360(5)	1.354(6)	1.364(3)	N8–C32–N11	107.1(3)	109.1(4)	108.7(2)
C9–N3	1.301(5)	1.323(6)	1.311(3)				
N3–C16	1.466(5)	1.485(6)	1.473(3)				
C16–N4	1.453(5)	1.459(6)	1.465(3)				
N4–C17	1.286(5)	1.272(6)	1.284(3)				
C17–N5	1.393(5)	1.408(6)	1.402(2)				
N5–C24	1.358(5)	1.363(5)	1.358(2)				
C24–N6	1.320(5)	1.318(6)	1.322(3)				
N6–C25	1.356(5)	1.337(7)	1.365(3)				
C25–N7	1.294(5)	1.315(6)	1.309(2)				

[a] D = Cl1 (**3a′**), O1D (**3b′**, κO-dmf) and O1 (**3aL**, κO-MeOH).[26]

are by far the shortest ones, see Table 4. These structural features are common to the other two helmet compounds discussed here, namely **3b** and **3aL**.[26] Moreover, such short bonds as observed for N4–C17/N8–C1 cannot be found in **4a** as all bonds are here aromatic in character. The more pronounced aromatic character of **4a** compared to **3a′** and **2b** can be checked by a further comparison of analogous bonds. The average bond lengths of C1–C2 and its analogous and symmetry generated equivalents amounts to 1.4525(11) Å. For **3a′** a significantly larger value of 1.4775(13) Å is observed, whereby the two pure single bonds C15–C16/C31–C32 were excluded from averaging, which displays less pronounced aromatic character. This tendency is even more pronounced in **2b**, the precursor of both **4a** and **3a′**, as the averaged bond lengths is here 1.493(4) Å.

^{1}H NMR spectroscopy of 3a and 3b

The compounds **3a–d** are all diamagnetic; but due to solubility reason, well-resolved ^{1}H NMR spectra could be recorded only for **3a** and **3b** in DMF-d_7 and CD_2Cl_2, respectively (see ESI for details†). The ^{1}H NMR spectra provide evidence for their C_2 symmetry in solution. Noteworthy, for the Ni^{II}-containing alkoxy-substituted "antenna"-type phthalogens of **Type III** a related observation was made,[33,34] whereas for all further literature-known phthalogens (Fig. 1) no well-resolved NMR spectra were reported. The electronic ESI display in Fig. S25† the aliphatic and aromatic regions of ^{1}H NMR spectra of [**3a**(HCl)(dmf)]·2dmf in DMF-d_7, while Fig. S26† shows the ^{1}H and ^{13}C{H} NMR spectra of [**3a**(MeOH)]·2MeOH in CD_2Cl_2.

The ^{1}H NMR of [**3a**(HCl)(dmf)]·2dmf shows in the aliphatic region two sets of signals related to DMF-d_7 residual signals and of dmf as coordinating and packing solvent.[51] In the aromatic region a complex series of resonances is observed, corresponding to the twenty aromatic protons of [**3a**(HCl)(dmf)]·2dmf (see Table S1†). A more detailed assignment is, due to their complexity, not possible. However, well-resolved ^{1}H and ^{13}C{^{1}H} NMR spectra of [**3a**(MeOH)]·2MeOH were accessible from measurements carried out in CD_2Cl_2. The ^{1}H NMR pattern in the aromatic region, corresponding to 20 aromatic protons, could be interpreted by assuming a C_2 sym-

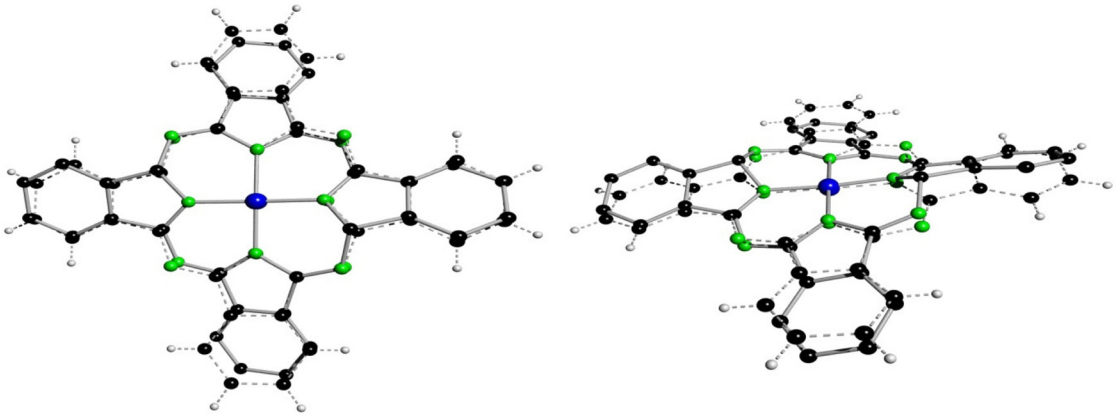

Fig. 6 Best fit of the $CoC_{32}N_8$ units of **4a** (dashed lines) onto the one of **3a'** (full line, hydrogen atoms omitted) in two different perspective views. All non-hydrogen atoms were used for fitting with the program XP.[50]

metry, which manifests additionally in the $^{13}C\{^1H\}$ NMR spectrum by 19 different resonances for the aromatic and one slightly upfield shifted resonance belonging to the sp^3-hybridized carbon atoms (Table S1†).

The full assignments of the protons and the carbon atoms was achieved with the aid of 2D homo- and heteronuclear NMR techniques (^1H–^1H COSY, ^1H–^{13}C HSQC, ^1H–^{13}C HMBC and ^1H–^{13}C HSQC-TOCSY (Fig. S27–S30†)). As part of this assignment the ^1H NMR resonances of H19 and H20 and the ^{13}C NMR signals of C17 to C20 belonging to the bridging "helm" was straightforward. However, the assignment of the NMR resonances belonging to the atoms of the $C_{32}H_{16}N_8$ core was more complicated, whereby the shifts of H11/C11 to H14/C14 could be assigned as belonging to the same chain *via* COSY techniques. However, a final assignment of the order of the atoms within the chain, even with the help of NOE-based 1D and 2D NMR techniques (NOESY, ROESY) based on an expected nuclear-overhauser-effect between H6 and H11, was not possible. On the contrary, C_2 symmetric **3b** displays in its ^1H NMR spectra five singlets only, corresponding to its ten aromatic protons. Due to the poorer solubility of **3b** compared to **[3a(HCl)(dmf)]·2dmf** and **[3a·MeOH]·2MeOH**, ^{13}C NMR measurements did not lead to evaluable results.

ESI-MS spectrometry of 3a–d

The four phthalogens **[3a(HCl)(dmf)]·2dmf**, **[3b(dmf)]·(dmf)·H_2O**, **[3c(HCl)]·dmf** and **[3d(MeOH)]·dmf** were characterized further by ESI-TOF-HRMS, whereby the insets displayed in Fig. 7 show the experimentally obtained isotope patterns of the fragments $[\mathbf{3a}–HCl–3dmf + H]^+$ (m/z = 714.1440, $^{12}C_{40}{}^1H_{21}{}^{54}Co^{14}N_{11}$), $[\mathbf{3b}–2dmf–H_2O + H]^+$ (m/z = 1053.7411, $^{12}C_{40}{}^1H_{11}{}^{35}Cl_{10}{}^{54}Co^{14}N_{11}$), $[\mathbf{3c}–HCl–dmf + H]^+$ (m/z = 854.2917, $^{12}C_{50}{}^1H_{41}{}^{54}Co^{14}N_{11}$) and $[\mathbf{3d}–MeOH–dmf + H]^+$ (m/z = 1014.2383, $^{12}C_{50}{}^1H_{41}{}^{54}Co^{14}N_{11}{}^{16}O_{10}$), confirming their molecular structure identities.

All peaks are isotopically resolved and are in agreement with their calculated isotopic patterns. The labile axial ligands (chloride in the case of **3a**, **3c**; dmf in the case of **3b** and MeOH in case of **3d**); as well as dmf packing solvents, are appears to dissociate from the complexes **3a–d** under the conditions of the mass spectrometric measurements (Fig. S31, S35, S37 and S40†).

IR spectroscopy of 3a–d

The FT-IR spectra in the range between 500–4000 cm^{-1} of **3a–d** are displayed in Fig. S32, S33, S36, S39 and S41, while the assignment of selected vibrational frequencies is given in Table S2.† Accordingly, sp^2 C–H stretching vibrations (rings), were observed for all compounds between 3094 and 3008 cm^{-1}, while the spectral range from 3000 to 2800 cm^{-1} is governed by C–H (sp^3) symmetric and asymmetric stretching vibrations,(ν_{as}(C–H) and ν_s(C–H) absorptions) of either the dmf methyl groups in all **3a–d** complexes or by the aliphatic substituents R of **3c** (R = CH_3) and **3d** (R = OCH_3). The presence of dmf is indicated further by the presence of carbonyl absorption band (ν(C=O) vibrations) at 1664 cm^{-1}, 1652 cm^{-1}, 1660 cm^{-1} and 1661 cm^{-1} for **3a–d**, respectively. The lower frequency of **3b** compared to **3a**, **3c** and **3d** is attributed to the different nature of dmf. Thereby, **3b** possesses a datively bonded dmf molecule, while in case of **3a**, **3c** and **3d** dmf acts as packing solvent. The ν(C=O) vibrations overlap partially with the ν(C=N) stretching vibrations and a large number of further aromatic ν(C=C) or ν(C=N) absorptions adds substantial complication for a more precise assignment.[24] Moreover, the absorptions at 1607, 1615, 1598 and 1603 cm^{-1} for **3a–d**, respectively, might be attributed to skeletal C–C vibrations (1580–1610 cm^{-1}).[24,52] A high intensity band at 1533, 1534, 1532 and 1533 cm^{-1} correlate to the vibrations of nitrogen bridging atoms (–N=).[52] In the range of 1430–1480 cm^{-1}, a bands varies in intensity; from low to high, were observed and attributed to the ν(C–C) stretching vibrations of isoindole skeleton (vibrations of the pyrrole and benzene residues).[52] The absorptions between 720 and 780 cm^{-1} for **3a–d**, are attributed to out-of-plane C–H bending of the arylic groups. The number of arylic C–H is for **3b–d** much smaller (with 10 aromatic C–H) as compared to **3a** (20 aromatic C–H). This difference is nicely

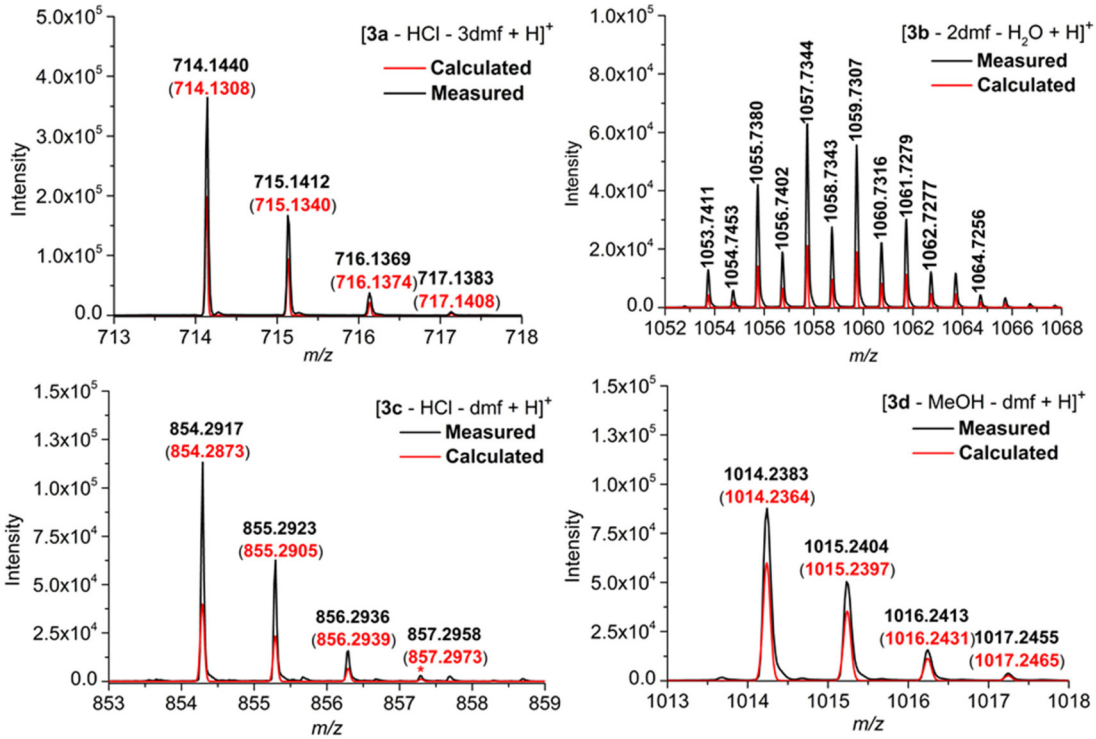

Fig. 7 Enlarged part of the HRMS (ESI-TOF) spectra of **3a–d** of the mole peak region.

reflected in the intensities and shapes of C–H absorptions (see ESI† for further details).[24,52]

UV/Vis spectroscopy of 3a, 3b and 3d

The UV/Vis spectra of **3a**, **3b** and **3d** (Fig. 8) display impressively the non-aromatic nature of the "helmet" type phthalogens compared to their Co^{II}-containing phthalocyanine counterparts, as the typical intense *Q* and Soret band of the latter are not observed. The principal features of the spectra are then consistent with the one reported for **3a** by McGaff and Sorokin.[26,30]

Initially, all three phthalogens **3a**, **3b** and **3d** exhibit similar features in their spectra. For **3a** intense bands at 234 and 248 nm and another band at 318 nm followed by two shoulders at 388 nm and at approximately 472 nm were observed. For **3b** we distinguish intense band at 262 nm, with a shoulder at 243 nm, a band at 318 nm followed by two shoulders at 398 and 475 nm respectively, while **3d** displays an intense band at 272 nm with a shoulder at 251 nm, a band at 323 nm and a shoulder at 384 nm (*cf.* Fig. S47–49 and Tables S4–6† for more details).

The intense higher energy bands observed around 248, 262 and 272 nm for **3a**, **3b** and **3d** respectively, might be due to π

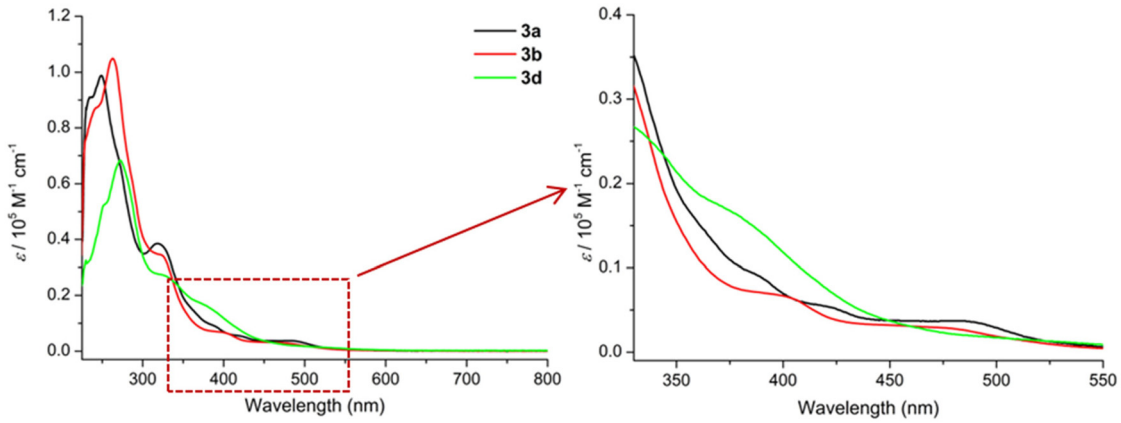

Fig. 8 UV/Vis spectra (CH_2Cl_2, 220–800 nm) of **3a** (c = 1.1333 × 10^{-5} M, black), **3b** (c = 1.6576 × 10^{-5} M, red), and **3d** (c = 2.1422 × 10^{-5} M, purple).

→ π* transitions of phenolic group within the ligand.[53] Based on Goutermann's and Lever's assignments,[54,55] the shoulders between 380 and 480 nm; which contains two in the case of **3a** and **3b** and one in the case of **3d**, were assigned to metal-to-ligand (MLCT) or ligand-to-metal (LMCT) charge-transfer transitions. Noticeable, absorptions solely based on d–d absorptions are not observed at all.[56]

Thermal behaviour of 2a–d

The thermal behaviour of **2a–d** in the solid state was studied by thermogravimetry (TG) and by differential scanning calorimetry (DSC). The appropriate TG traces are depicted in Fig. 9. The thermal decomposition of **2a** takes place in two steps (Fig. 9), but before decomposition melting at 140 °C is observed (Fig. S21†).

The onset temperature of the first decomposition of **2a** is 200 °C and this endothermic process is finished at 339 °C to leave a residue of 20.4%. This agrees well with a compound of the sum formula "CH_3N" (theoretical residue: 20.0%). There are two chemical species possessing this formula, namely methylenimine ($H_2C{=}NH$),[57] and the carbene aminomethylene ($H{-}C|{-}NH_2$).[58] While the latter specie could be isolated by matrix techniques at 12 K only,[58] methylenimine is available by gas phase pyrolysis of methylamine (CH_3NH_2) at 1000 °C, but is only stable within the gas phase.[57] Methylenimine is, however, unstable towards polymerization on surfaces[57] and much likely the residue obtained out of **2a** corresponds to $(H_2C{=}NH)_n$. However, this residue decomposes to gaseous reaction products or sublimes with an onset temperature of 511 °C to leave no residue in the TGA crucible (Fig. S21†).

In case of **2b** no melting is observed and the first endothermic decomposition occurred between 166 and 253 °C (Fig. 9 and S22†) to leave a mass residue of 93.2%. Most likely this decomposition liberates NH_3, leading to the formation of H_2PcCl_8 in analogy to urea melt reactions using 4,5-dichlorophthalic acid or related starting compounds.[39f] The theoretical mass residue for the formation of the phthalocyanine H_2PcCl_8 is with 91.8% close to the experimentally observed one. However, an exclusive tetra-cyclization of **2b** is unlikely and pristine-like phthalocyanines have in general a higher thermal stability[39f] compared to the second endothermic decomposition of **2b** in the range of 268–298 °C leaving 74.2% mass residue. The first decomposition is regarded as a fusion of **2b** to form higher oligomers (*e.g.* an hexamer, *cf.* Fig. S22†), while the nature of the second and third decomposition, starting at 345 °C (Fig. 9 and S22†), remains unknown.

Compound **2c** decomposes in a first endothermic decomposition in the temperature range of 214–289 °C (onset: 281 °C; Fig. 9 and S23†) to leave a mass residue of 32.7%. This agrees well with a compound of sum formula "C_3H_7N", which would correspond to, *e.g.*, acetone imine (theoretical mass loss 32.9%). In analogy to **2a** this hypothetical intermediate of **2c** is highly reactive and prone to polymerization,[59] and much likely "C_3H_7" compares therefore rather to a polymer of acetone imine. In a subsequent endothermic thermal decomposition at 340–460 °C a further mass loss to 23.0% is observed, which would correspond to a further decomposition of the "C_3H_7N" intermediate to a "C_2N" species corresponding to a theoretical mass loss of 22.0%. While, for compound **2d** in form of **2d**·H_2O adduct no melting is observed and the first mass loss between 57 and 96 °C (onset: 80 °C,, *mass loss*: theoretical: 8.1%, experimental: 9.7%; Fig. 9 and S24†), is due to the desorption of H_2O.[60] The nature of the second and third endothermic thermal decomposition, starting at 162 °C with a mass loss of 3.7%; (Fig. 9 and S24†), leaving 86.4% mass residue remains unknown. A further exothermic thermal decomposition in the range between 229–306 °C (onset: 279 °C, Fig. 9 and S24†) is observed; to leave a mass residue of 42.9%. This agrees well with a compound of the sum formula of "C_5H_5NO" (theoretical mass residue 42.6%).

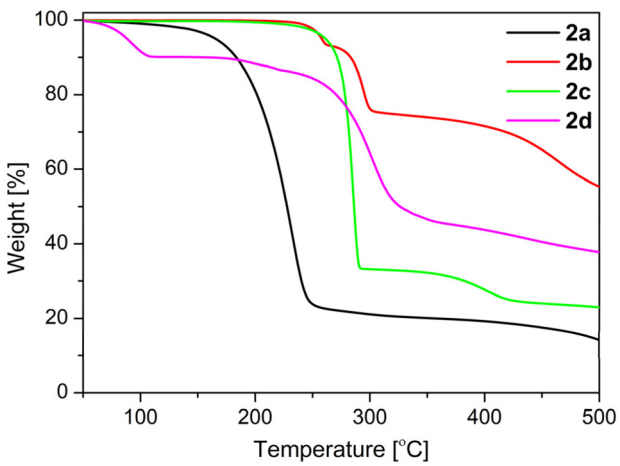

Fig. 9 TGA traces of **2a–d** under argon (40–500 °C, heating rate: 10 K min^{-1}, Ar gas flow: 20 ml min^{-1}).

Thermal behaviour of 3a–d

The thermal decomposition of **3a–d** phthalogens occurs in multistep process with several endothermic processes, as shown in Fig. 10 and S42–S46.† The onset temperatures and all further temperature ranges are summarized in Table S3.† Initially, for the phthalogens **3a–d** the mass decline at lower temperatures, precisely, for **3a** between 65 and 205 °C, for **3b** between 77 and 126 °C, for **3d** between 75 and 148 °C, is attributed to the loss of packing or coordinating solvents, as well as HCl (Fig. 10, S42–46 and Table S3†), depending on the nature of the investigated phthalogens, while for **3c** no mass declines were observed in these ranges.

Rising the temperature for **3a–d** a noticeable mass decline at 306–407 °C (**3a**), of 215–291 °C (**3b**), 256–301 °C (**3c**) and 245–263 °C for **3d** is observed. This mass decline is due to the "cleave off" or the release of the bridged diiminoisoindolino units, thus of the "helm".[11] The weight loss of the phthalogens **3a–d** fits to this assumption (Table S3†).

In order to confirm this both **3a** and **3b** were subjected to heating in a temperature-controlled furnace. The heating process consisted of two stages, whereby in step one the temperature was raised slowly (5 °C min^{-1}) to 380 °C and in step two this temperature was left constant for 2 hours, giving rise

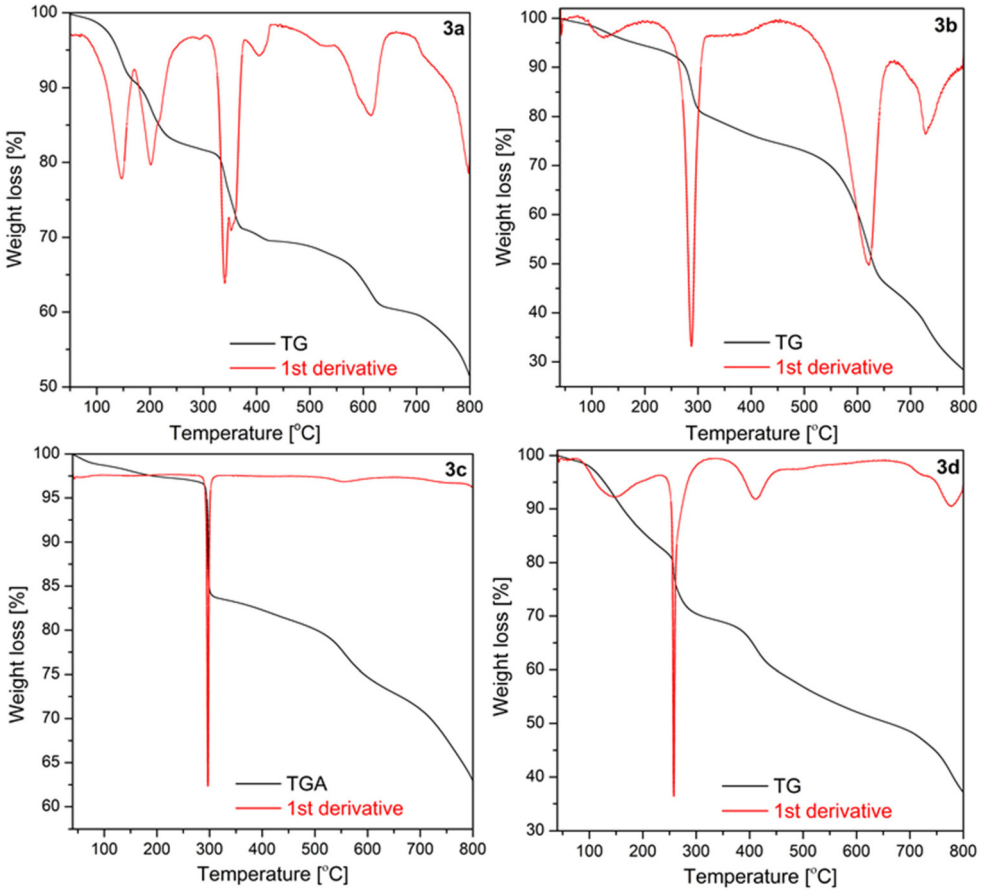

Fig. 10 TGA traces of **3a–d** under argon (40–800 °C, heating rate: 10 K min^{-1}, Ar gas flow: 20 ml min^{-1}).

to bright blue-coloured residues. Afterwards it was allowed to cool down to room temperature slowly (5 °C min^{-1}). The comparative FT-IR analysis of the obtained residues of **3a** and **3b** (Fig. 11, S51 and S52†), accompanied with a subsequently further thermogravimetric characterization (Fig. S53, S54 and S55†) confirmed them to correspond to the cobalt(II)-containing phthalocyanines **4a** (CoPc) and **4b** ($CoPcCl_8$). For example, the IR spectra of **4a** and of **4b** obtained by the two different chemical approaches compares well with each other as well as with already reported IR spectra.[39f]

After the "helms" of **3a–d** are cleaved-off to give the parent cobalt(II)-phthalocyanines **4a–d** the further mass decline is due to the thermal decomposition of the latter. This becomes obvious when comparing especially the TG traces of **3a** and **3b** with results reported of **4a** and **4b**.[39f]

Electrochemistry

The redox properties of phthalogens have been so far just sparingly described.[11] In order to shed more light on this topic the electrochemical properties of **3a** were determined and will be discussed compared to the ones of **4a**.[61] Therefore, **3a** was studied electrochemically by cyclic voltammetry (CV) and square wave voltammetry (SWV) in anhydrous DMF solutions containing 0.1 mol L^{-1} of $[N(^nBu)_4][B(C_6F_5)_4]$ as supporting electrolyte.[62] The data of the CV experiments of **3a** at a scan rate of 100 mV s^{-1} are summarized in Table 5.

The cyclic voltammogram of **3a** (Fig. 12) clearly displays three irreversible reduction process at −1319 mV (E^1_{pc}) (**Ia**) and −1550 mV (E^2_{pc}) (**Ib**) and −1754 mV (E^3_{pc}) (**II**). They are followed by four quasi-reversible one-electron reductions at −1919 mV ($E^\circ_1{}'$) (**III**), −1975 mV ($E^\circ_2{}'$) (**IV**), −2075 ($E^\circ_3{}'$) (**V**) and −2454 mV ($E^\circ_4{}'$) (**VI**) during the cathodic scan. The processes (**III–V**) take place in a very close potential range and they are not resolvable by CV; nonetheless, the SWV confirms the exiting of three processes (Fig. 12, inset). In the anodic scan an additional one-electron oxidation at −953 mV is observed ($E^\circ_5{}'$) (**VII**).

There are noticeable differences in the electrochemical processes between the initial and the 1st cycle (Fig. 12, left). The reduction processes **Ia**/**Ib** of the initial cycle are not observed in the 1st cycle, while this cycle comprises a reduction process denoted as # in Fig. 12. Measuring up to the 5th full cycle reveals no further changes compared to the observations made for the 1st cycle (Fig. 12, right). The slight decline in current in due course of the 1st to the 5th indicates that the material generated electrochemically in the initial cycle remains stable throughout the applied potential range.

These observations are interpreted as follows: in the initial cycle the reduction processes **Ia** and **Ib** are due to the $Co^{III/II}$

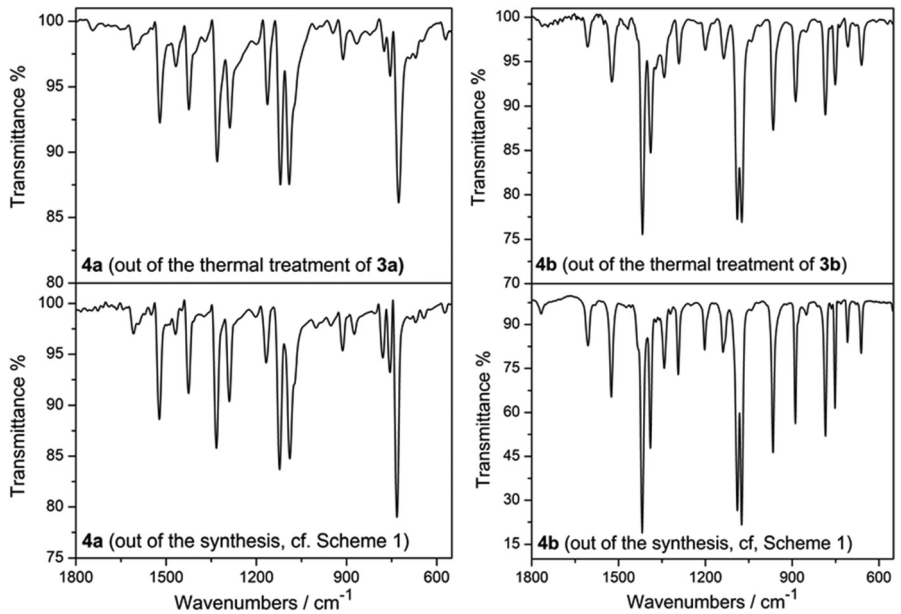

Fig. 11 IR spectra of **4a**/**4b** obtained out of thermal treatment of **3a**/**3b** (left/right, above) and of **4a**/**4b** obtained by work-up according to Scheme 1 (left/right, below) in the region of 550–1800 cm^{-1}.

Table 5 CV data of **3a** in the range of 0 to −2750 mV. All potentials are given in [mV]

Couple	$E^{\circ\prime}$ [a] [mV]	ΔE_p [b] [mV]
Ia	−1319[c]	—
Ib	−1550[c]	—
II	−1754[c]	—
III	−1919[d]	—
IV	−1975[d]	—
V	−2075 [d]	—
VI	−2454	81
VII	−953	70

[a] $E^{\circ\prime}$ = formal potential = $((E_{pa} + E_{pc})/2)$. [b] $\Delta E_p = (E_{pa} - E_{pc})$. [c] E_{pc} = cathodic peak potential of the irreversible process. [d] Values taken from the square-wave voltammogram.

reduction of **3a**, followed by the cleavage of the helm by two one electron bond breaking processes of the two N–C_{sp^3} bonds. These two reductions, however, convert **3a** to **4a** (CoPc). This conversion is electrochemically irreversible, as it was already shown to be chemically irreversible.[10] Subsequently a reduction at −1754 mV and a set of reductions (**III–VI**, Fig. 12, and Table 5) is observed. They are attributed to a $Co^{II/I}$ reduction and four reductions of the phthalocyanato core, as already reported.[61] The same electrochemical behaviour of **3a** has been observed using a glassy carbon working electrode (Fig. S66, and Table S8†).

Experimental section

Reagents and materials

1,2-Dicyanobenzene (phthalonitrile), 1,2-dimethylbenzene, 1,2-dimethoxybenzene and 4,5-dichlorophthalonotrile were purchased from TCI Chemical and used as received. Ammonia (NH_3) solution (7 M in methanol (MeOH)) and sodium methoxide (NaOMe) solution (0.5 M in MeOH) were purchased from Sigma-Aldrich and used as received. Extra dry MeOH (99.8%, over Molecular Sieve, AcroSeal®) and extra dry *N,N*-dimethylformamide (DMF), (99.8%, AcroSeal®) were purchased from Acros Organics and used as received. 1,2,4-Trichlorobenzene was purchased from Acros Organics and used as received. Cobalt(II) chloride hexahydrate, 98% was purchased from Alfa Aesar (Johnson Matthey company) and used as received. The solvents were purified and dried using standard methods prior to use.[63] Dichloromethane (CH_2Cl_2) was dried with an MBraun MB SPS-800 system (double column solvent filtration, working pressure 0.5 bar) and further purified by distillation from calcium hydride.[63] Tetrahydrofuran (THF) was distilled prior to use. 1,2-Dibromo-4,5-dimethylbenzene,[64] 4,5-dimethylphthalonitrile,[65] 1,2-dibromo-4,5-dimethoxybenzene,[66] 4,5-dimethoxyphthalonitrile,[65] and $[N(nBu)_4][B(C_6F_5)_4]$,[67] were synthesized in accordance with literature procedures. Column chromatography was performed on *silica gel* with a particle size of 200–300 mesh. Columns were packed as slurry of *silica gel* in *n*-hexane or CH_2Cl_2 and equilibrated solution using the appropriate solvent system.

Apparatus and measurements

Proton nuclear magnetic resonance (^1H NMR) and carbon NMR ($^{13}C\{^1H\}$ NMR) were recorded in DMSO-d_6; otherwise stated, at ambient temperature using a Bruker Avance III 500 Ultra Shield Spectrometer in the Fourier transform mode. The spectra were recorded at 500.300 MHz (^1H), 125.813 MHz ($^{13}C\{^1H\}$), respectively. The chemical shifts δ are reported in ppm, using the residual solvent signal as an internal standard:

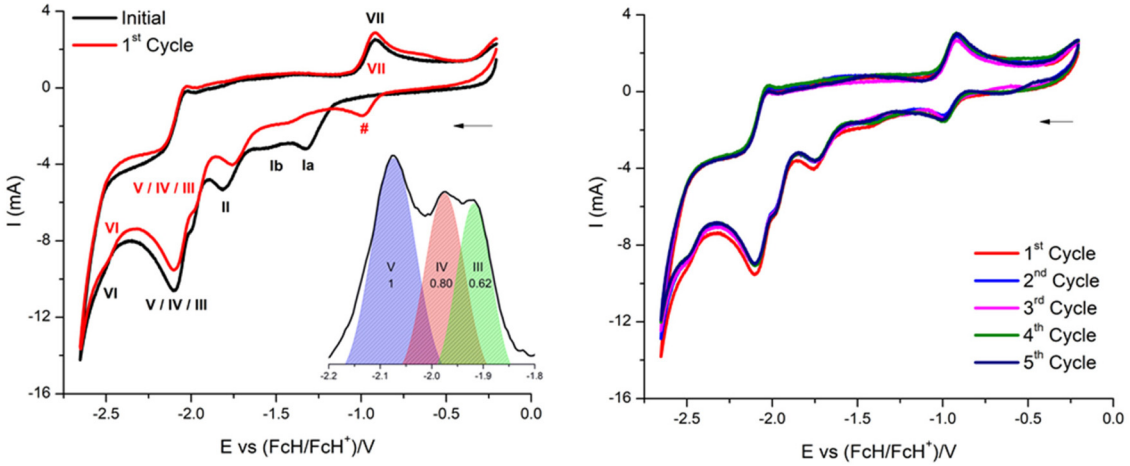

Fig. 12 Left: cyclic voltammograms of **3a**; inset: the square-wave voltammogram of **3a** (duration 5 s, amplitude 5 mV, pulse 25 mV); right: set of cyclic voltammograms of **3a**. Scan rate: 100 mV s^{-1}; in DMF solutions (1.0 mmol L^{-1}) at 25 °C, supporting electrolyte 0.1 mol L^{-1} of $[N(nBu)_4][B(C_6F_5)_4]$, working electrode: platinum electrode. Roman numbers in black correspond to processes in the initial and in red to the 1st cycle.

($CDCl_3$: ^1H NMR, δ = 7.26 ppm, $^{13}C\{^1H\}$ NMR, δ = 77.16 ppm); (DMSO-d_6: ^1H NMR, δ = 2.50 ppm; and $^{13}C\{^1H\}$ NMR, δ = 39.52 ppm); (DMF-d_7: ^1H NMR, δ = 2.75, 2.92 ppm, $^{13}C\{^1H\}$ NMR, δ = 29.76, 34.89 ppm); (CD_2Cl_2: ^1H NMR, δ = 5.32 ppm, $^{13}C\{^1H\}$ NMR, δ = 53.84 ppm). Multiplicities were given as: s (singlet), d (doublet), t (triplet), q (quartet), m (multiplets), dd (doublet of doublets), dt (doublet of triplets), and br (broad). A Bruker Avance 400 spectrometer equipped with double-tuned probes capable of MAS (magic angle spinning) was used to record the solid-state NMR spectra (^1H-MAS NMR (400.1 MHz) and $^{13}C\{^1H\}$ CP-MAS NMR (100.6 MHz)). Spinning 3.2 mm zirconium oxide rotors are used for sample packing at 15 kHz. ^1H-MAS NMR was obtained with single pulse excitation (90° pulse, pulse length 2.4 μs) and a recycle delay of 6 s. Cross-polarization (CP) technique with a contact time of 3 ms is used to enhance sensitivity for acquiring the spectra. The $^{13}C\{^1H\}$-CP-MAS NMR is collected with ^1H decoupling using a TPPM (two-pulse phase modulation) pulse sequence with a 6 s recycle delaying. The spectra are referenced to tetramethylsilane using TTSS (tetrakis(trimethylsilyl)silane) as an internal secondary standard (3.55 ppm for ^{13}C, 0.27 ppm for ^1H). Infrared spectroscopy (FT-IR) studies in solid state using KBr disc were performed in the range of 400–4000 cm^{-1} using a PerkinElmer 1000 FT-IR spectrometer. Bands are characterized as broad (br), strong (s), medium (m), and weak (w). C,H,N elemental analyses were performed using a Thermo FlashAE 1112 series analyzer. High resolution electrospray ionization mass spectrometry HRMS (ESI-TOF) were recorded in units of mass of charge ratio (m/z) with a Bruker micrOTOF QII equipped with an Apollo II ESI source. Mass samples were dissolved in DMF/MeCN or DMSO/MeCN or CH_2Cl_2/MeCN (HPLC grade). Ultraviolet/visible (UV/Vis) absorption spectra were recorded using a Spectronic GENESYS 6 UV/Vis spectrophotometer (Thermo Electron Corporation) between 200–800 nm. TG experiments were performed using a Mettler Toledo TGA/DSC 11600 system with a MX1 balance. The melting points of **2a–d** were determined by a Gallenkamp MFB 595 010 M melting point apparatus.

Electrochemical measurements were performed with 1.0 mmol L^{-1} solutions of the analytes in anhydrous DMF solutions containing 0.1 mol L^{-1} of $[N(nBu)_4][B(C_6F_5)_4]$ as supporting electrolyte under a blanket of purified argon at 25 °C. The instrumentation consists of a Radiometer Voltalab PGZ 100 electrochemical workstation interfaced with a personal computer. The measurement cell contains three electrodes, a Pt auxiliary electrode, a glassy carbon working electrode (surface area 0.031 cm^2), and an Ag/Ag^+ (0.01 mol L^{-1} $AgNO_3$) reference electrode. The working electrode was pretreated by polishing on a Buehler microcloth subsequently with 1 μm and 1/4 μm diamond paste. The reference electrode was constructed from a silver wire inserted in a 0.01 mmol L^{-1} $AgNO_3$ and a 0.1 mol L^{-1} $[N(nBu)_4][B(C_6F_5)_4]$ MeCN solution in a luggin capillary with a Vycor tip. This luggin capillary was inserted into a second luggin capillary with a Vycor tip filled with a 0.1 mol L^{-1} $[N(nBu)_4][B(C_6F_5)_4]$ in DMF. Under these conditions all experiments showed that all oxidation and reduction processes were reproducible in the range of ±5 mV. All experimental potentials were internally referenced against a Ag/Ag^+ reference electrode, whereas all presented results are referenced against FcH (as internal standard) as recommended by IUPAC.[49,68] When Fc* [Fc* = $Fe(\eta^5\text{-}C_5Me_5)_2$] was used as an internal standard, the experimentally measured potential was converted into *E vs.* FcH/FcH^+ (under our conditions the Fc^*/Fc^{*+} couple was at −614 mV *vs.* FcH/FcH^+, ΔE_p = 60 mV).[69] Data were then manipulated with a Microsoft Excel worksheet to set the formal redox potential of the FcH/FcH^+ couple to 0 V.

Single crystal X-ray diffraction studies

Data of **2b**, **3a**, **3b** and of **4a** were collected with a Rigaku Oxford Gemini S diffractometer, while the one of **2c** were col-

lected with a Bruker Venture D8 diffractometer. All structures were solved by direct methods and refined by full-matrix least-squares procedures on (F^2)[70] as implemented in the WINGX v2013.3 suite.[71] All non-hydrogen atoms were refined anisotropically and all carbon-bonded hydrogen atoms isotropically by using appropriate riding models. The atomic positions of nitrogen-bonded hydrogens were taken from Difference Fourier Maps and refined freely and isotropically. Crystallographic data have been deposited with Cambridge Crystallographic Data Centre: CCDC 2298395 (**2b**), 2298396 (**2c**), 2298397 (**3a**), 2298398 (**3b**) and 2298399 (**4a**).†

Theoretical calculations

ORCA[72] was employed for structure optimizations in the gas phase and in DMF solution in combination with the spin-component scaled second-order Møller–Plesset perturbation theory (SCS-MP2)[73] and the aug-cc-pVTZ basis set.[74,75] The resolution of identity approximation was employed to speed up the Hartree–Fock (RI-JK)[76–79] as well as the SCS-MP2 part (RI-MP2[80,81]) of the calculation. Solvation effects were considered by the conductor-like polarizable continuum model (C-PCM).[82] TURBOMOLE[83] was used to obtain thermodynamic corrections. This includes the following steps: structure optimization employing the BP86 functional[84,85] and the TZVP basis set.[86] Seminumerical frequency calculation employing NumForce. Subsequently, thermodynamic corrections were calculated by freeh, a tool provided by Turbomole. All calculations with TURBOMOLE employed the RI-approximation[76,77,87] and solvation effects were considered by the conductor like screening model (COSMO).[88]

General synthetic procedure for 3a–d and 4a–d

The 1,3-diiminoisoindoline's **2a–d** were synthesized from the corresponding phthalonitriles **1a–d** as described in detail in the ESI.† For the synthesis of **3a–d** to a 500 mL one-neck (ground glass joint, NSH 29) round bottom flask containing a suspension of the corresponding 1,3-diiminoisoindolines **2a–d** (5 equiv.) in 1,2,4-trichlorobenzene (150 mL), $CoCl_2{\cdot}6H_2O$ (1 equiv.) was added in a single portion at ambient temperature. Afterwards, a *ca.* 30 cm long reflux condenser (NSK 29) was mounted, and the reaction mixture temperature was raised slowly to 80 °C (within 1 h) under permanent stirring. Then, from 80 °C on, the heating rate was reduced (20 °C per 2 h), and the reaction mixture was heated gradually up to 210 °C. Noteworthy, by reaching *ca.* 100–120 °C NH_3 was developed. The mixture was then heated at 210 °C as long as the NH_3 development was noticed (heating may take up to 5 days). After the NH_3 gas development had stopped, the reaction mixture was allowed to cool down to ambient temperature, filtrated and washed with CH_2Cl_2 (40 mL). The filter cake was next treated with DMF to separate between **3a–d** and **4a–d**. Out of crystallizations, dark red or orange-red crystals were grown by slow diffusion of et_2O into DMF solution, which were identified as **3a–d**. Crystals were collected, washed first with small amount of DMF then *n*-hexane, air dried in a fume hood and were used without further purification unless specified. While, the violet filter cake; which was identified later as the corresponding cobalt(II)phthalocyanines (**4a–d**), was washed first with DMF (5 × 30 mL) until no further green color, then washed with freshly distilled THF (4 × 50 mL) and air dried; (see ESI for full details†).

Conclusions

In this paper we have demonstrated that the synthesis of the "helmet"-type phthalogens **3a–d** with a rather broad variation of their substituents is possible *via* the use of 1,3-diiminoisoindolines (**2a–d**) as precursors. This synthetic route is easy-to-follow and affords the phthalogens in much higher yields compared to so far reported synthetic routes and makes this unique member of the porphyrinoid family broadly accessible beyond lab curiosities. With this larger set of pentadenate "helmet" phthalogens thermal decomposition studies were performed which verified that the "helms" are cleaved-off to give the parent cobalt(II)-containing phthalocyanines **4a–d**. Furthermore, it was shown for **3a** as example that a related cleavage occurs electrochemically. Besides potential applicability of **3a–d** in homogenous catalytic oxidation reactions the easy accessibility of these precursors of metallophthalcyanines offers now a broader use of them for engineering optical media, coloured fibres or other material science application. Our future work is devoted to the synthesis of further series of "helmet"-type phthalogens with different metal centre.

Conflicts of interest

There are no conflicts to declare.

Acknowledgements

This work was supported by the Deutsche Forschungsgemeinschaft through project FOR 1154 "Towards Molecular Spintronics". R. K. Al-Shewiki and S. W. thank FOR 1154 for a grant. Solid state NMR spectroscopic measurements were carried out by Dr Andreas Seifert at the Polymer chemistry department of the Technical University of Chemnitz. S. Z. is grateful to the Center for Information Services and High Performance Computing [Zentrum für Informationsdienste und Hochleistungsrechnen (ZIH)] for providing its facilities for computational studies.

References

1 For examples, see: (*a*) B. D. Berezin, *Coordination Compounds of Porphyrins and Phthalocyanines*, Wiley, Chichester, 1981; (*b*) N. B. McKeown, *Phthalocyanine materials: Synthesis, Structure and Function*, Cambridge University Press, 1998; (*c*) C. C. Leznoff and A. B. P. Lever, *Phthalocyanines: Properties and Applications*, Wiley-VCH,

New York, 1989, 1993, 1993, 1996; (*d*) *The porphyrin handbook*, ed. K. M. Kadish, K. M. Smith and R. Guilard, Academic, San Diego, 2003; (*e*) M. S. Rodriguez-Morgade, G. de la Torre and T. Torres, in *The Porphyrin Handbook*, Academic Press, New York, 2003, pp. 125–160.

2 For examples, see: (*a*) W. M. Sharman and J. E. van Lier, in *The Porphyrin Handbook*, Academic Press, New York, 2003; 15, 1–60; (*b*) N. B. McKeown, in *The Porphyrin Handbook*, Academic Press, New York, 2003, pp. 61–124; (*c*) K. Sakamoto and E. Ohno-Okumura, *Materials*, 2009, **2**, 1127–1179; (*d*) V. N. Nemykin and E. A. Lukyanets, *ARKIVOC*, 2010, 136–208; (*e*) E. A. Lukyanets and V. N. Nemykin, *J. Porphyrins Phthalocyanines*, 2010, **14**, 1–40; (*f*) D. Arıcan, M. Arıcı, A. L. Ugur, A. Erdogmus and A. Koca, *Electrochim. Acta*, 2013, **106**, 541–555.

3 For examples, see: (*a*) Y. Chen, M. Hanack, W. J. Blau, D. Dini, Y. Liu, Y. Lin and J. Bai, *J. Mater. Sci.*, 2006, **41**, 2169–2185; (*b*) D. Dini, M. Calvete and M. Hanack, *Chem. Rev.*, 2016, **116**, 13043–13233.

4 Y. C. Tsai, *U.S. Pat. Appl* US 20060292494A1 20061228, 2006.

5 (*a*) C. G. Claessens, U. Hahn and T. Torres, *Chem. Rec.*, 2008, **8**, 75–97; (*b*) M. G. Walter, A. B. Rudine and C. C. Wamser, *J. Porphyrins Phthalocyanines*, 2010, **14**, 760–792; (*c*) D. Wöhrle, G. Schnurpfeil, S. G. Makarov, A. Kazarin and O. N. Suvorova, *Macroheterocycles*, 2012, **5**, 191–202; (*d*) Y. Matsuo, K. Ogumi, I. Leon, H. Wang and T. Nakagawa, *RSC Adv.*, 2020, **10**, 32578–32689.

6 For examples, see: (*a*) M. Gsänger, D. Bialas, L. Huang, M. Stolte and F. Würthner, *Adv. Mater.*, 2016, **28**, 3615–3645; (*b*) M. L. Esqueda, M. E. S. Vergara, J. R. Á. Bada and R. Salcedo, *Materials*, 2019, **12**, 434–451.

7 (*a*) Z. Z. Öztürk, N. Kılınça, D. Atilla, A. G. Gürek and V. Ahsen, *J. Porphyrins Phthalocyanines*, 2009, **13**, 1179–1187; (*b*) M. Bouvet, P. Gaudillat and J.-M. Suisse, *J. Porphyrins Phthalocyanines*, 2013, **17**, 913–919; (*c*) T. Kerdcharoen and S. Kladsomboon, in *Applications of Nanomaterials in Sensors and Diagnostics*, 2013, pp. 237–255.

8 T. Nyokong, *Pure Appl. Chem.*, 2011, **83**, 1763–1779.

9 J. H. Zagal, S. Griveau, J. F. Silva, T. Nyokong and F. Bedioui, *Coord. Chem. Rev.*, 2010, **254**, 2755–2791.

10 F. Baumann, B. Bienert, G. Rösch, H. Vollmann and W. Wolf, *Angew. Chem.*, 1956, **68**, 133–150, and patents cited therein.

11 H. Lang and T. Rüffer, *Applications of Porphyrinoids as functional materials*, The royal Society of Chemistry, CPI group, UK, 2021.

12 F. Gund, *J. Soc. Dyers Colour.*, 1953, **69**, 671–682.

13 C. Ercolan, A. M. Paoletti, G. Pennesi, G. Rossi, A. Chiesi-Villa and C. Rizzoli, *J. Chem. Soc., Dalton Trans.*, 1990, 1971–1977.

14 M. P. Donzello, C. Ercolani and P. J. Lukes, *Inorg. Chim. Acta*, 1997, **256**, 171–172.

15 M. P. Donzello, C. Ercolani, A. Chiesi-Villa and C. Rizzoli, *Inorg. Chem.*, 1998, **37**, 1347–1351.

16 E. M. Bauer, M. P. Donzello, C. Ercolani, E. Masetti, S. Panero, G. Ricciardi, A. Rosa, A. Chiesi-Villa and C. Rizzoli, *Inorg. Chem.*, 2003, **42**, 283.

17 J. Janczak and R. Kubiak, *Polyhedron*, 2003, **22**, 313.

18 J. Janczak and R. Kubiak, *J. Porphyrins Phthalocyanines*, 2017, **21**, 1.

19 F. Gingl and J. Strähle, *Acta Crystallogr., Sect. C: Cryst. Struct. Commun.*, 1990, **46**, 1841–1843.

20 J. Janczak and R. Kubiak, *J. Chem. Soc., Dalton Trans.*, 1994, 2539–2543.

21 J. Janczak and R. Kubiak, *Acta Crystallogr., Sect. C: Cryst. Struct. Commun.*, 1995, **51**, 2039–2042.

22 J. Janczak and R. Kubiak, *Acta Chem. Scand.*, 1995, **49**, 871–877.

23 K. Benihya, M. Mossoyan-Deneux, F. Hahn, N. Boucharat and G. Terzian, *Eur. J. Inorg. Chem.*, 2000, 1771.

24 K. Benihya, M. Mossoyan-Déneux and M. Giorgi, *Eur. J. Inorg. Chem.*, 2001, 1343–1352.

25 T. Fukuda, N. Shigeyoshi, A. Fuyuhiro and N. Ishikawa, *Dalton Trans.*, 2013, **42**, 16486–16489.

26 H. M. Kieler, M. J. Bierman, I. A. Guzei, P. J. Liska and R. W. McGaff, *Chem. Commun.*, 2006, 3326–3328.

27 E. S. Brown, J. R. Robinson, A. M. McCoy and R. W. McGaff, *Dalton Trans.*, 2011, **40**, 5921–5925.

28 B. M. Peterson, M. E. Herried, R. L. Neve and R. W. McGaff, *Dalton Trans.*, 2014, **43**, 17899–17903.

29 R. L. Neve, M. C. Eidenschink, I. A. Guzei, B. M. Peterson, G. M. Vang and R. W. McGaff, *ChemistrySelect*, 2016, **1**, 5182–5186.

30 I. Y. Skobelev, E. V. Kudrik, O. V. Zalomaeva, F. Albrieux, P. Afanasiev, O. A. Kholdeeva and A. B. Sorokin, *Chem. Commun.*, 2013, **49**, 5577–5579.

31 R. W. McGaff, *U. S. Pat*, US 10065980B2, 2018.

32 R. W. McGaff, WO 2020/041284A1, 2020.

33 C. D. Molek, J. A. Halfen, J. C. Loe and R. W. McGaff, *Chem. Commun.*, 2001, 2644–2645.

34 J. R. Robinson, K. A. Bahr, M. J. Bierman, I. A. Guzei, H. M. Kieler-Ferguson, A. M. McCoy and R. W. McGaff, *Dalton Trans.*, 2011, **40**, 11809–11814.

35 Y. Y. Karabach, M. N. Kopylovich, K. V. Luzyanin, M. F. C. Guedes da Silva, V. Yu. Kukushkin and A. J. L. Pombeiro, *Inorg. Chim. Acta*, 2016, **455**, 696–700.

36 Y. Kikukawa, T. Fukuda, A. Fuyuhiro, N. Ishikawa and N. Kobayashi, *Chem. Commun.*, 2011, **47**, 8518–8520.

37 T. Fukuda, Y. Kikukawa, R. Tsuruya, A. Fuyuhiro, N. Ishikawa and N. Kobayashi, *Inorg. Chem.*, 2011, **50**, 11832–11837.

38 T. Fukuda, Y. Kikukawa, A. Fuyuhiro, N. Kobayashi and N. Ishikawa, *Chem. Lett.*, 2014, **43**, 925–927.

39 For examples, see: (*a*) J. A. Elvidge and R. P. Linstead, *J. Chem. Soc.*, 1952, 5000–5007; (*b*) J. A. Elvidge and R. P. Linstead, *J. Chem. Soc.*, 1952, 5008–5012; (*c*) P. F. Clark, J. A. Elvidge and R. P. Linstead, *J. Chem. Soc.*, 1953, 3593–3601; (*d*) J. A. Elvidge and R. P. Linstead, *J. Chem. Soc.*, 1955, 3536; (*e*) P. J. Brach, S. J. Grammatica, O. A. Ossanna and L. Weinberger, *J. Heterocycl. Chem.*,

1970, **7**, 1403; (*f*) T. Rüffer, D. Nurpeisova, Z. Jakupova, A. Tashenov, N. Uhlig, A. Khalladi, L. Mertens, A. Gonser, M. Mehring and H. Lang, *Z. Naturforsch., B: J. Chem. Sci.*, 2017, **72**, 589–601.

40 (*a*) C. G. Claessens, D. Gonzalez-Rodriguez and T. Torres, *Chem. Rev.*, 2002, **102**, 835–853; (*b*) T. Torres, *Angew. Chem., Int. Ed.*, 2006, **45**, 2834–2837; (*c*) A. Medina and C. G. Claessens, *J. Porphyrins Phthalocyanines*, 2009, **13**, 446–454.

41 (*a*) F. Fernandez-Lazaro, T. Torres, B. Hauschel and M. Hanack, *Chem. Rev.*, 1998, **98**, 563–575; (*b*) W. S. Durfee and C. J. Ziegler, *J. Porphyrins Phthalocyanines*, 2009, **13**, 304–311.

42 (*a*) W. O. Siegl, *Inorg. Chim. Acta*, 1977, **25**, L65–L66; (*b*) W. O. Siegl, *J. Heterocycl. Chem.*, 1981, **18**, 1613–1618; (*c*) W. O. Siegl, *J. Org. Chem.*, 1977, **42**, 1872–1878.

43 (*a*) A. B. P. Lever, B. S. Ramaswamy and S. R. Pickens, *Inorg. Chim. Acta*, 1980, **46**, L59–L61; (*b*) L. K. Thompson, V. T. Chacko, J. R. Elvidge, A. B. P. Lever and R. V. Parish, *Can. J. Chem.*, 1969, **47**, 4141–4152; (*c*) A. B. P. Lever, L. K. Thompson and W. M. Reiff, *Inorg. Chem.*, 1972, **11**, 104–109.

44 (*a*) H. Hopff and P. Gallegra, *Helv. Chim. Acta*, 1968, **51**, 253–260; (*b*) R. Sato, T. Senzaki, Y. Shikazaki, T. Goto and M. Saito, *Chem. Lett.*, 1984, 1423–1426.

45 O. V. Shishkin, I. S. Konovalova, R. I. Zubatyuk, G. V. Palamarchuk, S. V. Shishkina, A. V. Biitseva, I. V. Rudenko, V. A. Tkachuk, M. Yu. Kornilov, O. V. Hordiyenko and J. Leszczynski, *Struct. Chem.*, 2013, **24**, 1089–1097.

46 A. Acker, H.-J. Hofmann and R. Cimiraglion, *J. Mol. Struct.*, 1994, **315**, 43–51.

47 A. V. Lyubimtsev, A. Baranski, M. K. Isayaikin and R. P. Smirnov, *Chem. Heterocycl. Compd.*, 1997, **33**, 937–941.

48 Zh.-Q. Zang, J. M. Njus, D. J. Sandman, C. Guo, B. M. Foxman, P. Erk and R. Van Gelder, *Chem. Commun.*, 2004, **5**, 886–887.

49 J. T. Engle, A. N. Allison, J. M. Standard, I.-S. Tamgho and C. J. Ziegler, *J. Porphyrins Phthalocyanines*, 2013, **17**, 1–10.

50 *XP 'A graphical program'. VS. SHELXTL-5.0*, Bruker AXS GmbH.

51 L. Wang, L. Lin, G. Zhang, K. Kodama, M. Yasutake and T. Hirose, *Chem. Commun.*, 2014, **50**, 14813–14816.

52 A. V. Ziminov, S. M. Ramsh, E. I. Terukov, I. N. Trapeznikova, V. V. Shamanin and T. A. Yurre, *Semiconductors*, 2006, **40**, 1131–1136.

53 D. K. Rastogi, S. K. Sahnis, V. B. Rana and S. K. Dua, *J. Coord. Chem.*, 1918, **8**, 97–104.

54 P. Sayer, M. Gouterman and C. R. Connell, *Acc. Chem. Res.*, 1982, **15**, 73–79.

55 A. B. P. Lever, S. R. Pickens, P. C. Minor, S. Licoccia, B. S. Ramaswamy and K. Magnell, *J. Am. Chem. Soc.*, 1981, **103**, 6800–6806.

56 *Inorganic Electronic Spectroscopy*, A. B. P. Lever, American Elsevier publishing company, New York, 1968, pp. 299–314.

57 R. Pearson Jr. and F. J. Lovas, *J. Chem. Phys.*, 1977, **66**, 4149–4156.

58 A. K. Eckhardt and P. R. Schreiner, *Angew. Chem., Int. Ed.*, 2018, **57**, 5248–5252.

59 J. M. Casas, J. Fornies, A. Martin and A. J. Rueda, *Organometallics*, 2002, **21**, 4560–4563.

60 E. Pousaneh, M. Korb, V. Dzhagan, M. Weber, J. Noll, M. Mehring, D. R. T. Zahn, S. E. Schulze and H. Lang, *Dalton Trans.*, 2018, **47**, 10002–10016.

61 (*a*) D. W. Clark, N. S. Hush and I. S. Woolsey, *Inorg. Chim. Acta*, 1967, **19**, 129–132; (*b*) A. Koca, H. A. Dincer, M. B. Kocak and A. Gül, *Russ. J. Electrochem.*, 2006, **42**, 31–37.

62 W. E. Geiger and F. Barrière, *Acc. Chem. Res.*, 2010, **43**, 1030–1039.

63 D. D. Perrin and W. L. F. Armarego, *Purification of Laboratory Chemicals, Vol. 3*, Pergamon, New York, 1988.

64 A. V. Ivanov, K. V. Kabanova, M. O. Breusova, I. V. Zhukov, L. G. Tomilova and N. S. Zefirov, *Russ. Chem. Bull.*, 2008, **57**, 1665–1670.

65 Z. Iqbal, A. Lyubimtsev and M. Hanack, *Synlett*, 2008, 2287–2290.

66 L. Babel, T. N. Y. Hoang, L. Guenee, C. Besnard, T. A. Wesolowski, M. Humbert-Droz and C. Piguet, *Chem. – Eur. J.*, 2016, **22**, 8113–8123.

67 R. J. LeSuer, C. Buttolph and W. E. Geiger, *Anal. Chem.*, 2004, **76**, 6395–6401.

68 G. Gritzner and J. Kuta, *Pure Appl. Chem.*, 1984, **56**, 461–466.

69 (*a*) A. Nafady and W. E. Geiger, *Organometallics*, 2008, **27**, 5624–5631; (*b*) I. Noviandri, K. N. Brown, D. S. Fleming, P. T. Gulyas, P. A. Lay, A. F. Masters and L. Phillips, *J. Phys. Chem B*, 1999, **103**, 6713–6722; (*c*) J. Ruiz and D. Astruc, *C. R. Acad. Sci. Paris Ser. IIc.*, 1998, 21–27.

70 G. M. Sheldrick, *Acta Crystallogr., Sect. A: Found. Crystallogr.*, 2008, **64**, 112–122.

71 L. J. Farrugia, *J. Appl. Crystallogr.*, 2012, **45**, 849–854.

72 F. Neese, The ORCA program system, *Wiley Interdiscip. Rev.: Comput. Mol. Sci.*, 2012, **2**, 73–78.

73 S. J. Grimme, *Phys. Chem.*, 2003, **118**, 9095–9102.

74 T. H. Dunning Jr., *J. Chem. Phys.*, 1989, **90**, 1007–1023.

75 D. E. Woon and T. H. Dunning Jr., *J. Chem. Phys.*, 1993, **98**, 1358–1371.

76 E. J. Baerends, D. E. Ellis and P. Ros, *J. Chem. Phys.*, 1973, **2**, 41–51.

77 B. I. Dunlap, J. W. D. Connolly and J. R. Sabin, *J. Chem. Phys.*, 1979, **71**, 3396–3402.

78 F. Weigend, *Phys. Chem. Chem. Phys.*, 2002, **4**, 4285–4291.

79 F. Weigend, *Phys. Chem. Chem. Phys.*, 2006, **8**, 1057–1065.

80 M. Feyereisen, G. Fitzgerald and A. Komornicki, *Chem. Phys. Lett.*, 1993, **208**, 359–363.

81 F. Weigend, A. Köhn and C. Hättig, *J. Chem. Phys.*, 2002, **116**, 3175–3183.

82 V. Barone and M. Cossi, *J. Phys. Chem. A*, 1998, **102**, 1995–2001.

83 R. Ahlrichs, M. Bär, M. Häser, H. Horn and C. Kölmel, *Chem. Phys. Lett.*, 1989, **162**, 165–169.
84 A. D. Becke, *Phys. Rev. A*, 1988, **38**, 3098–3100.
85 J. P. Perdew, *Phys. Rev. B: Condens. Matter Mater. Phys.*, 1986, **33**, 8822–8824.
86 A. Schäfer, C. Huber and R. Ahlrichs, *J. Chem. Phys.*, 1994, **100**, 5829–5835.
87 K. Eichkorn, F. Weigend, O. Treutler and R. Ahlrichs, *Theor. Chem. Acc.*, 1997, **97**, 119–124.
88 A. Klamt and G. Schüürmann, *J. Chem. Soc., Perkin Trans. 2*, 1993, 799–805.